Environmental Research Center Papers

Number 1

1982

Environmental Research Center
The University of Tsukuba

PREFACE

Environmental Research Center of the University of Tsukuba is a research center for the study of various natural phenomena on and near the earth's surface, especially those studies related to geomorphology, hydrology, climatology and meteorology. The center is composed of two sections: a hydraulics section and heat and water balance section. Although construction of facilities is not yet complete, research and data acquisition is being actively pursued by the Center's staff and other users. The staff is composed of: 1 professor (joint appointment), 1 associate professor, 1 lecturer, 1 assistant, 5 technical assistants and 1 secretary.

The results have been published annually in the *Bulletin of the Environmental Research Center* in Japanese since 1977 and in *Observational Data of Heat Balance and Water Balance* since 1980. New series named *Environmental Research Center Papers,* which is written in English, is an irregular publication of a monographic work such as a doctoral thesis or a project report.

The two sections of the Environmental Research Center mentioned above have major facilities respectively: one is the large (4 m wide, 2 m deep and 160 m long) flume and the other one is the heat and water balance experimental field. Objectives of the large flume are: 1) to simulate the changing inclination of natural stream beds, 2) to simulate variations in textural proportions of bottom materials in natural beds, 3) to have the flowing water in the flume sufficiently deep so that turbulence can be examined, 4) to reduce the side friction of the flume to a minimum, 5) to conduct long-period experiments without interrupting the sediment or water supply, and 6) while achieving the above objectives, maintain a reasonable operating cost. The heat and water balance experimental field is facilitated by a grass covered field 160 m in diameter. At its center is a 30 m high meteorological observation tower. On the tower and in the field are number of instruments including: 1) sonic anemometer thermometers at 4 levels on the tower, 2) resistance thermometers at 3 levels, 3) dew point thermometers at 3 levels, 4) resistance thermometers at 4 levels in the ground, 5) heat flux plates at 2 levels in the ground, 6) groundwater level guages at 3 levels, 7) pyrheliometer, 8) total hemispherical radiometer, 9) net radiometer, 10) weighing lysimeter, 11) evaporation pan, 12) rainfall intensity recorder, 13) rain guage, and 14) discharge meter. The main purpose of this system is to acquire the long term basic data needed to aid in the understanding of the heat and water balance under natural conditions and to clarify the transfer processes of heat and water energy in and near the surface boundary layer.

It is our great pleasure to be able to contribute the respective research fields with these facilities. Number 1 of the *Environmental Research Center Papers* is a work on micrometeorology by Dr. K. Kai, analysing the values measured at the 30 m tower of the experimental field. We are expecting that the following Numbers will be published soon. Taking this opportunity, we wish to express our hearty thanks for his effort to accomplish the facilities of the Center during the beginning years to Professor Masao Inokuchi, former Director of the Center.

December 1981

Masatoshi M. Yoshino
Director of the Environmental
Research Center

[We send our publications for exchange purpose only]

STATISTICAL CHARACTERISTICS OF TURBULENCE AND THE BUDGET OF TURBULENT ENERGY IN THE SURFACE BOUNDARY LAYER*

By Kenji Kai

Environmental Research Center, the University of Tsukuba
Ibaraki, 305 Japan
(received 1 August 1981)

ABSTRACT

Turbulence measurements of wind and temperature were made by sonic anemometer-thermometers in the first thirty meters of the atmosphere. Direct measurements of turbulent fluctuations are possible to present the data in the context of the Monin-Obukhov similarity theory. This experiment has allowed a detailed study of the turbulent energy budget as well as turbulence statistics in the surface boundary layer.

Firstly, turbulence statistics are analyzed and interpreted in relation to measured parameters such as height, mean wind speed and stability conditions. The values for the friction velocity u_* increase linearly with the mean wind speed $\overline{U}$. The standard deviations of the velocity components have close relations to mean wind speed, friction velocity and stability. The data for the horizontal components are rather scattered in comparison with those for the vertical compenent. The normalized intensity of turbulence for the vertical component, σ_w/u_*, shows the dependence on the stability parameter z/L, and is given by a universal function of z/L according to the similarity theory. The values for σ_w/u_* in neutral conditions are in agreement with the results obtained by other investigators. The spectral analysis of turbulent fluctuations reveals that the spectra of the velocity components on the high-frequency side have the slope of $-5/3$ corresponding to Kolmogorov's hypothesis. The $-5/3$ region is assumed to be the inertial subrange, where the ratio between the spectra of the longitudinal component u and the vertical component w is found to be 4/3. In addition, the spectral analysis shows that the horizontal scale of turbulence is larger than the vertical one, and that the scale of turbulence increases with both height and stability, and decreases with the mean wind speed.

Secondly, terms in the budget equation of turbulent energy were derived from turbulence statistics, and their behaviors were examined. The vertical structure and time change of the turbulent energy budget are shown for unstable and stable conditions in comparison with the budget in the planetary boundary layer, obtained previously by other investigators. The behavior of each term in the budget equation was considered for a wide range of stability conditions.

The values for viscous dissipation were obtained from the inertial-subrange levels of the longitudinal velocity spectra with a value of 0.50 for the spectral constant. Viscous dissipation increases with the third power of mean wind speed at any height, and decreases with height. For

* Doctor of Science Thesis in the Institute of Geoscience, the University of Tsukuba.

unstable conditions, mechanical production and viscous dissipation of turbulent energy are a main energy source and sink, respectively. They decrease with height. Turbulent transport of turbulent energy is an energy sink to approximately balance buoyant production which may be a source or sink depending on stability. For stable conditions, the magnitude of each term is very small and almost constant with height.

Thirdly, a model of turbulent energy was deduced from the results, and presented in the context of the Monin-Obukhov similarity theory. A general specification of the turbulent energy budget including the case of stable conditions has been achieved through this model.

CONTENTS

LIST OF FIGURES

LIST OF TABLES

LIST OF SYMBOLS

A_i	Spectral constants for spectra of the velocity components (i = u, v, w)
BP	Buoyant production term in the turbulent energy budget
c_p	Specific heat for air at constant pressure
$\phi_B(z/L)$	Dimensionless term of buoyant production of turbulent energy
$\phi_\epsilon(z/L)$	Dimensionless viscous dissipation of turbulent energy
$\phi_I(z/L)$	Dimensionless term of the imbalance
$\phi_M(z/L)$	Dimensionless term of mechanical production of turbulent energy, or dimensionless wind shear
$\phi_T(z/L)$	Dimensionless term of turbulent transport of turbulent energy
ϵ	Viscous dissipation of turbulent energy
$F_i(z/L)$	Universal function of intensity of turbulence
f	Dimensionless frequency ($f = nz/\overline{U}$)
f_m	Dimensionless frequency at which $nS_w(n)/\sigma_w^2$ is a maximum
G	Undetermined dimensionless function of the spectrum
$G_{s.i.}$	Normalized spectra of longitudinal, lateral and vertical velocity components (i = u, v, w)
g	Acceleration due to gravity
H	Sensible heat flux ($H = c_p\rho\overline{w\theta} = -c_p\rho u_* T_*$)
IM	Imbalance term in the turbulent energy budget
k	Kármán constant ($k = 0.4$)
k_h	Turbulent diffusivity for heat
κ	Wavenumber ($\kappa = 2\pi n/\overline{U}$)
L	Monin-Obukhov length ($L = -(u_*^3\rho c_p\overline{T})/(kgH)$)
λ	Wavelength ($\lambda = \overline{U}/n$)
λ_m	Wavelength at which $nS_w(n)$ is a maximum ($\lambda_m = \overline{U}/n_m$)
MP	Mechanical production term in the turbulent energy budget
n	Frequency in Hz
$n_{i.s.}$	Frequency which is the lower limit of the inertial subrange
n_m	Frequency at which $nS_w(n)$ is a maximum
P	Instantaneous pressure ($P = \overline{P} + p$)
$\overline{P}$	Mean pressure
p	Fluctuating pressure ($\overline{p} = 0$)
PT	Pressure transport term in the turbulent energy budget
ρ	Air density
$\frac{1}{2}q^2$	Turbulent energy ($q^2 = u^2 + v^2 + w^2$)
ν	Kinematic viscosity
R_f	Flux Richardson number ($R_f = (g/\overline{T})\overline{w\theta}/(\overline{uw}\partial\overline{U}/\partial z)$)
R_i	Gradient Richardson number ($R_i = (g/\overline{T})\,(\partial\overline{T}/\partial z)/(\partial\overline{U}/\partial z)^2$)
θ	Fluctuating temperature ($\overline{\theta} = 0$)
$S_i(\kappa)$, $S_i(n)$	Spectra of the velocity components (i = u, v, w) with respect to wavenumber or frequency
σ_i	Standard deviations of the velocity components (i = u, v, w)

σ_i^2	Variances of the velocity components (i = u, v, w)
σ_T	Standard deviation of temperature
T	Instantaneous temperature ($T = \overline{T} + \theta$)
$\overline{T}$	Mean temperature
T_*	Scaling temperature for the surface boundary layer ($T_* = -H/(\rho c_p u_*)$)
t	Time
TT	Turbulent transport term in the turbulent energy budget
τ	Reynolds stress ($\tau = -\rho\overline{uw} = \rho u_*^2$)
(u, v, w)	Components of the turbulent wind vector ($\overline{u} = \overline{v} = \overline{w} = 0$)
(U, V, W)	Instantaneous velocity components in the longitudinal, lateral and vertical directions ($U = \overline{U} + u$, $V = \overline{V} + v$, $W = \overline{W} + w$)
$(\overline{U}, \overline{V}, \overline{W})$	Mean velocity components in the longitudinal, lateral and vertical directions
U_x	Instantaneous velocity component from the north
U_y	Instantaneous velocity component from the east
$\overline{U}_x$	Mean velocity component from the north
$\overline{U}_y$	Mean velocity component from the east
u_*	Friction velocity or scaling velocity for the surface boundary layer ($u_* = \sqrt{-\overline{uw}}$)
VD	Viscous dissipation term in the turbulent energy budget
WD	Mean wind direction
(x, y, z)	Cartesian coordinate system, x pointing either north or along mean wind, y lateral and z vertical
z_0	Roughness length
z/L	Monin-Obukhov stability parameter

CHAPTER 1

INTRODUCTION

1-1 Background of the study

Over the past two decades, there have been numerous experimental studies of profiles, fluxes, variances, spectra and other statistics of wind and temperature in the surface boundary layer. Since most of the transfer of momentum and heat is due to the turbulent fluctuations of wind and temperature, it seems obvious that the energy budgets of the fluctuations are important areas for study. The most important of these budgets is the budget of turbulent energy, which provides some information about the dynamics of these quantities in a turbulent flow.

It is helpful for understanding the budget concept to present the mathematical expression of the turbulent energy budget, which can be written for the case of horizontally homogeneous turbulence (see Lumley and Panofsky, 1964)

$$\underset{\text{(TE)}}{\frac{\partial}{\partial t}\frac{\overline{q^2}}{2}} = \underset{\text{(MP)}}{-\overline{uw}\frac{\partial \bar{U}}{\partial z}} + \underset{\text{(BP)}}{\frac{g}{\bar{T}}\overline{w\theta}} \underset{\text{(TT)}}{-\frac{\partial}{\partial z}\frac{\overline{wq^2}}{2}} \underset{\text{(PT)}}{-\frac{\partial}{\partial z}\frac{\overline{wp}}{\rho}} \underset{\text{(VD)}}{-\epsilon} \quad \cdots\cdots\cdots\cdots \quad (1\text{-}1)$$

where u, v, w are the three components of the wind fluctuation ($\overline{u} = \overline{v} = \overline{w} = 0$) in directions x, y, z, respectively; $\bar{U}$ is the mean wind speed; θ, p are the fluctuating temperature and pressure, respectively; $q^2 = u^2 + v^2 + w^2$ is twice the turbulent energy per unit mass; $\bar{T}$ and ρ are the means of temperature and density; and ϵ is the rate of viscous dissipation of turbulent energy. The terms in Eq. (1-1) can be identified as (from the left) the instantaneous turbulent energy TE, mechanical production MP, buoyancy production BP, turbulent transport TT, pressure transport PT, and viscous dissipation VD. Brief interpretation of these terms is as follows:

TE: the local rate of change of turbulent energy, which is zero for steady-state conditions.

MP: mechanical production of turbulent energy by the Reynolds stress, which is normally positive.

BP: thermal production of turbulent energy by the buoyancy forces, which is positive under unstable conditions and negative under stable conditions.

TT: turbulent transport, or the divergence of turbulent energy.

PT: pressure transport, or the divergence of the rate of working by the pressure forces.

VD: transformation of turbulent energy to heat by the viscous forces.

Fig. 1-1 shows a schematic diagram of the turbulent energy budget.

1-2 Purpose of the study

There are three purposes of this study. The first is to analyze and interpret turbulence statistics in relation to measured parameters, such as height, wind speed and stability conditions. The second is to investigate the time change and vertical structure of the turbulent energy budget. The third purpose, the main one, is to make a model of the turbulent energy budget over a wide range of stability conditions by means of the similarity theory proposed by Monin and Obukhov (1954), which explains the behavior of each term in the budget equation in relation to stability.

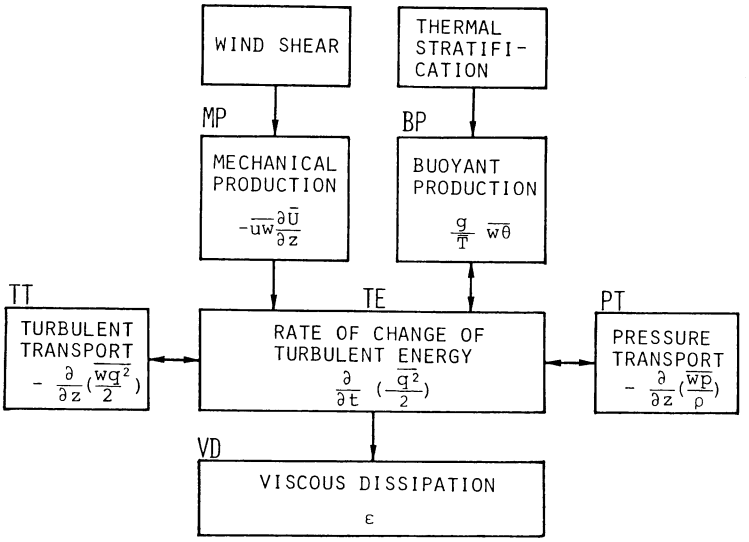

Fig. 1-1 Schematic diagram of the turbulent energy budget.

In order to carry out these purposes, turbulence measurements of wind and temperature were made in the first thirty meters of the atmosphere. Four sonic anemometer-thermometers were used for turbulence measurements. This experiment has allowed a detailed study of the turbulent energy budget in the surface boundary layer. In the present study it is possible to make measurements of all terms except the pressure transport term in the budget, allowing a quantitative determination of the terms over a wide range of stability conditions.

1-3 Review of the recent research

Since the early 1960's, when modern instrumental, recording and computing techniques became available, the small-scale structure of atmospheric turbulence has been the subject of extensive research. Numerous experiments were carried out in order to obtain a comprehensive set of data on wind and temperature fluctuations in the lowest thirty meters, or so, of the planetary boundary layer. Most of the results were systematically analyzed, using the framework of similarity which was put forward originally by Obukhov (1946). The first experimental evidence for the similarity theory was given by Monin and Obukhov (1954). The Monin-Obukhov similarity theory permitted a concise representation of the effects of stability. These previous efforts made it possible to predict the general behavior of atmospheric turbulence described in terms of simple turbulence statistics to a fair degree of accuracy. Previous studies were reviewed thoroughly in the books by Lumley and Panofsky (1964), Haugen (1973) and Pasquill (1974).

Theoretical studies have shown qualitative characteristics of turbulence to a certain degree, but not for quantitative ones. Experimental studies are necessary for acquiring information with regard to the quantitative characteristics. Since the main purpose of the present study is to establish a model of the turbulent energy budget, this review will be limited to the experimental studies concerning these experiments, as summarized in Table 1-1. Since Panofsky (1962) suggested that the budget concept is useful for presenting dynamic effects of turbulent fluctuations, there have

Table 1-1 Summary of various experiments associated with the turbulent energy budget.

Observer	Location	Type of terrain	Height of measurement (m)	Sensor	Averaging time (sec)	Duration (min)	Stability	Comments
Panofsky, 1962	Brookhaven, N.Y.	Scrub pine	23,46,91	Aerovane Bivane	5	60	All	
McBean et al., 1971	Vancouver	Mown grass	2	SAT Hot-wire	0.0125	15	Unstable Neutral	
Wyngaard & Coté, 1971	Kansas	Uniform wheat	5.66, 11.3, 22.6	SAT Hot-wire	0.05	60	Unstable	T.E.B. model
Garratt, 1972	Lough Neagh, Northern Ireland	Over water	1.4, 4, 12	Bivane Hot-wire	0.1	15	All	ϵ vs. z/L
Monji, 1973	Bonneville, Utah	Salt crystal	4.2, 15	SAT Thermocouple		40	Unstable	
McBean & Elliott, 1975	Suffield, Alberta	Prairie grass	5.77	SAT	0.05	250	Unstable Neutral	Spectral model
Rayment & Caughey, 1977	Earles Croome, England	Rural	61, 91, 152	Cardington turbulence probe		120	Unstable	Time change
Maitani, 1977	Kojima Bay	Paddy field	1.2, 3	SAT	0.17	30	Unstable	
Yamamoto, 1977	Kawaguchi	Urban	20, 45, 90, 180, 313	SAT	0.05-2.5	8.3-40	Stable	
This study	Tsukuba	Grass about 50 cm tall	1.6, 4.3, 12.3, 29.5	SAT	0.05	30(90)	All	T.E.B. model Time change Vertical structure

been several experimental studies on the turbulent energy budget in the surface boundary layer (Panofsky, 1962; Busch and Panofsky, 1968; Wyngaard and Coté 1971; etc.). In spite of these experimental studies, there is still not complete agreement on the relative importance of each term in the budget equation.

Panofsky (1962) stated that the flux of turbulent energy was upward and that turbulent transport was an important term in the budget equation under unstable conditions. Busch and Panofsky (1968), however, concluded that viscous dissipation was balanced by mechanical and buoyant productions and that turbulent transport was unimportant in the case of a homogeneous terrain.

Instrumented aircrafts were used to estimate directly the budget of turbulent energy in the planetary boundary layer by Lenschow (1970, 1974). Lenschow (1970) reported that viscous dissipation was almost constant with height between the lowest flight level of 100 m above the ground, and the highest flight level of 1,000 m, which was just below the top of the planetary boundary layer, while turbulent transport increased with height to balance the decrease in buoyant production. Lenschow (1974) proposed a model of the height variation of the turbulent energy budget in the unstable planetary boundary layer.

In 1968, the Air Force Cambridge Research Laboratories carried out an extensive experiment of the surface boundary layer at a site in Kansas (Haugen, 1973); one outcome of this experiment was the paper by Wyngaard and Coté (1971) on the budgets of turbulent energy and temperature variance, as shown in Fig. 1-2. The study was the most complete that has ever been reported. Wyngaard and Coté showed that the turbulent energy budget in the surface boundary layer appeared to follow the Monin-Obukhov similarity theory quite well. Under stable conditions, viscous dissipation essentially balanced mechanical production, while turbulent transport was of secondary importance. Under unstable conditions, viscous dissipation exceeded the total of mechanical and buoyant productions by a significant amount and turbulent transport was important. The large imbalance among the measured terms in the budget under unstable conditions was discussed. The cause of the imbalance could not be determined with certainty, but an interesting possibility was that pressure transport was significant under very unstable conditions.

McBean et al. (1971) reported that for slightly unstable conditions the total production was

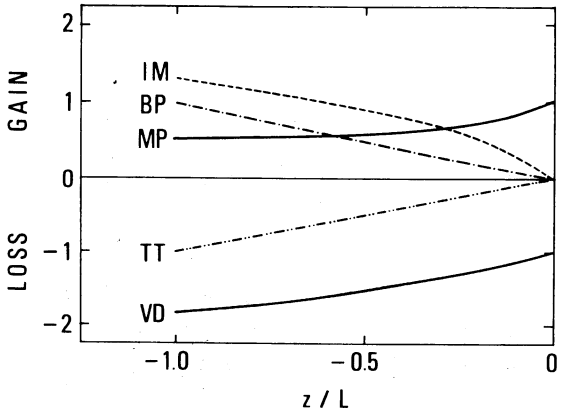

Fig. 1-2 Dimensionless energy budget under unstable conditions (from Wyngaard and Coté, 1971).

balanced by viscous dissipation and that for more unstable conditions viscous dissipation exceeded the production. Garratt (1972) found that viscous dissipation and turbulent transport was significant on occasions but small on the average. From the standpoint of the budget relations of turbulent energy and temperature variance, Monji (1973) discussed the transition from the surface layer to the free convection layer of the unstable planetary boundary layer. Maitani (1977) showed the characteristics of the turbulent transport and viscous dissipation were the main loss terms under unstable conditions and that these terms increased in magnitude with increasing instability.

The imbalance (or residual) of the budget equation can be attributed either to pressure transport or to experimental difficulties such as horizontal inhomogeneity. Conclusions from recent experiments have tended to confirm the existence of the imbalance and have more closely identified this with pressure transport. Pressure transport has been measured directly only by Elliot (1972). He constructed and tested an instrument for measuring pressure fluctuations within the surface boundary layer. His results indicated that pressure transport was about one-tenth of mechanical production for near neutral conditions, but no measurements were made for stable and unstable conditions. It is possible that pressure transport could be more important under unstable conditions. McBean and Elliott (1975) examined the transport of turbulent energy by turbulence and pressure for a surface boundary layer over a dry prairie grassland. They found that for unstable condition turbulent transport was about equal to minus buoyant production, and that pressure transport was of opposite sign and of about equal magnitude to turbulent transport.

The 1968 Kansas experiment was unique in providing direct measurements of all terms except pressure transport in the budget. Wyngaard and Coté established the model of the turbulent energy budget for unstable conditions, but a general specification of the turbulent energy budget including the case of stable conditions has not yet been achieved (Fig. 1-2). The emphases in this study will be on the behavior of the turbulent energy budget under stable conditions as well as under unstable conditions.

CHAPTER 2

EXPERIMENTAL METHODS

This experiment was designed to deduce each term in the budget equation of turbulent energy from the measurements of turbulence statistics and their profiles. This chapter describes the essential details of the experiment, including the experimental site, instrumentation, data collection and reduction. The detailed descriptions have been given by Kotoda et al. (1978) and Kai (1978).

2-1 Experimental site and instrumentation

The site is the hydrometeorological observation field of Environemntal Research Center, the University of Tsukuba, at Sakura-mura, Ibaraki-ken, Japan (36° 05′ N, 140° 06′ E; see Fig. 2-1). Fig. 2-2 shows a view of the site and the 30 m tower. The field is circular in shape with a radius of 80 m and is covered by grass about 50 cm tall. The neighboring area is not completely homogeneous due to some buildings and forests. This implies that terms in the budget arising from horizontal inhomogeneity could perhaps be significant on occasion and that deductions about the nature of the imbalance quantities must be considered somewhat tentative.

The 30 m tower was built at the center of the circular field. Fig. 2-3 shows a horizontal cross section of the 1 m square lattice-type tower with boom arrangements for the sonic anemometers

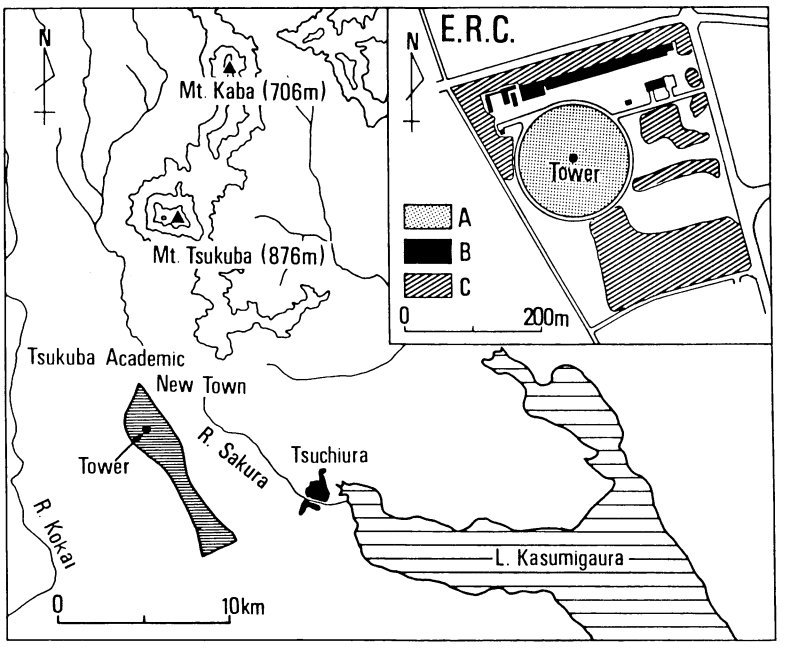

Fig. 2-1 Location of the experimental site. A = Grass field, B = Buildings, C = Coniferous wood.

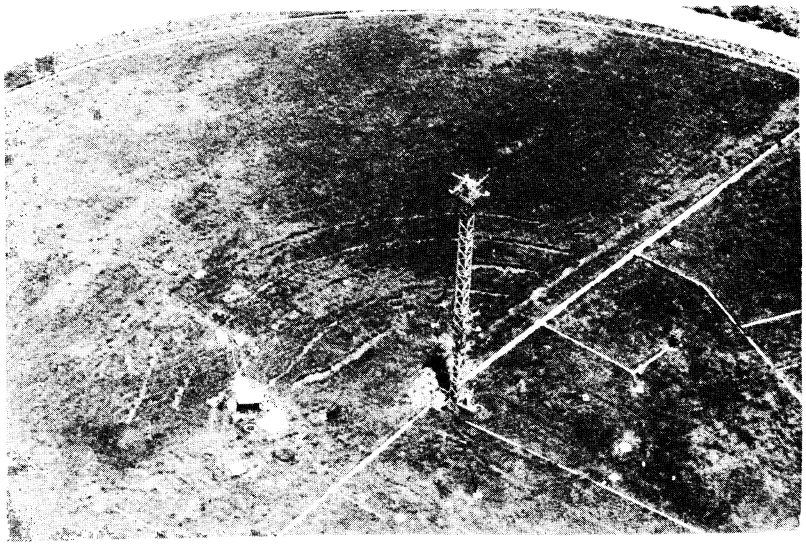

Fig. 2-2 View of the experimental site.

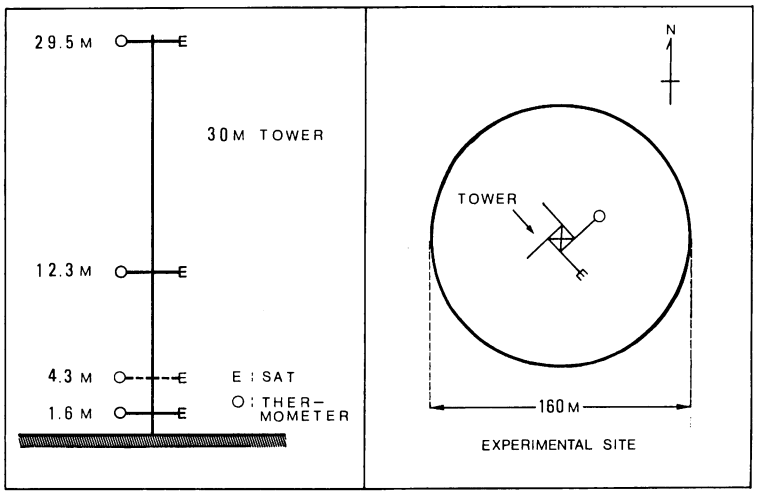

Fig. 2-3 30 m tower and the arrangement of sensors.

and the resistance thermometers at the levels of 1.6, 4.3, 12.3 and 29.5 m above the ground. The booms for the four sonic anemometers extended 2.0 m to southeast. The desired wind direction for data collection was from southeast, to avoid distorting influences of the tower structure on the wind sensors. The booms for the resistance thermometers extended 2.0 m to northeast.

Fluctuating velocity components and temperature fluctuations were measured with three-component sonic anemometer-thermometers (Kaijō Denki Model PAT 311). The sonic anemometer has become a prime research instrument for turbulent velocity measurements in the atmosphere. A collection of studies on the development, comparison and use of this instrument is given by Mitsuta (1966, 1971). Mitsuta (1966) employed the propagation of a sound wave in order to

measure the velocity and temperature of the atmosphere. The operation of the sonic anemometer is based on the dependence of the transit time of the sound pulse propagating between source and receiver transducers on the velocity component along the path of known length as shown in Fig. 2-4. Usually two parallel paths with pulses propagating in opposite directions are used, and the difference between the transit times is approximately proportional to the velocity vector component averaged over the path length. The sensing head of the anemometer has three 20 cm sound paths to measure the wind, one for the vertical component and two for the horizontal components. The frequency response of the sensors is about 20 Hz. The high wavenumber response is limited by averaging over the 20 cm sound paths of the probe, but is adequate to measure spectra up to a frequency of 10 Hz. Electronic zero and full-scale adjustments were recorded on magnetic tapes in the same format as the field data. A computer was programmed to calculate calibration coefficients.

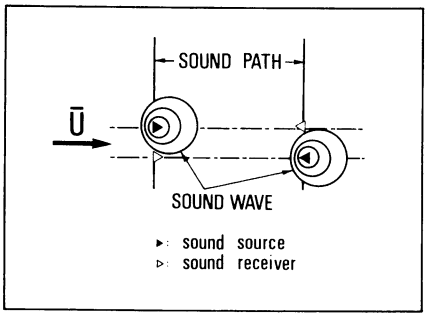

Fig. 2-4 Diagram showing the principle of the sonic anemometer-thermometer operation.

Mean profiles of wind and temperature were measured with sonic anemometers and resistance thermometers at 1.6, 4.3, 12.3 and 29.5 m (Figs. 2-5 and 2-6). Solar radiation was measured with a pyranometer, net radiation with a net radiometer, and heat flux into the soil with a heat flux plate embedded 2 cm below the ground.

Fig. 2-7 shows a block diagram for the entire experimental system. The output signals from these sensors were transmitted through cables to a building outside the field and recorded on a computer-controlled data acquisition system (Kaijō Denki Model GP-1100), which consists of a analog-to-digital converter, a multiplexor for multichannel analysis, a microcomputer for system control and a magnetic tape unit (Fig. 2-8). The signals were continuously monitored on chart recorders.

2-2 Data collection and reduction

The experimental runs are listed in Table 2-1. Data collection was restricted to periods when the wind was mainly from southeast and constant in speed and direction. An experimental period was terminated when either wind speed or direction became unfavorable, i.e., to avoid the tower influence on wind speed measurements and the effect of nonstationarity.

A typical run length was 90 min, occasionally shortened to 10, 30 or 60 min during the actual experiment or during subsequent analyses. The basic averaging period used for the statistical analyses was 10 min. The mean and linear trends were removed from the turbulent velocity and

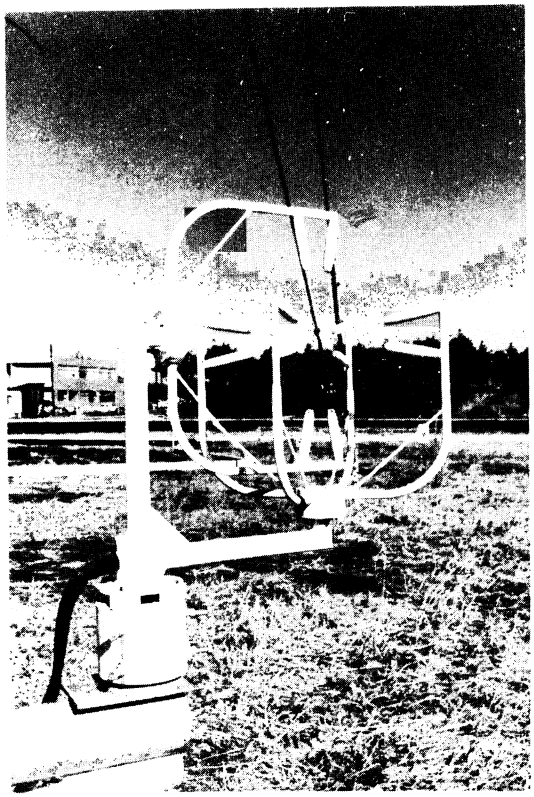

Fig. 2-5 View of the sensor probe of the sonic anemometer-thermometer.

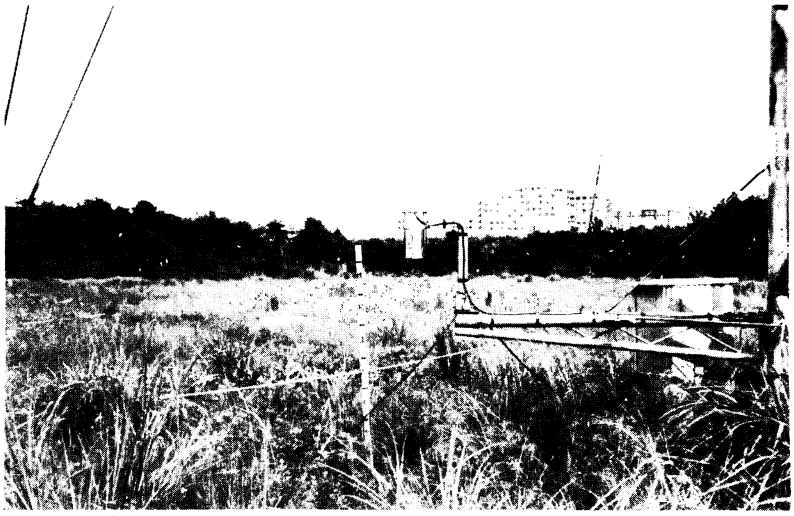

Fig. 2-6 View of the sensor probe of the resistance thermometer.

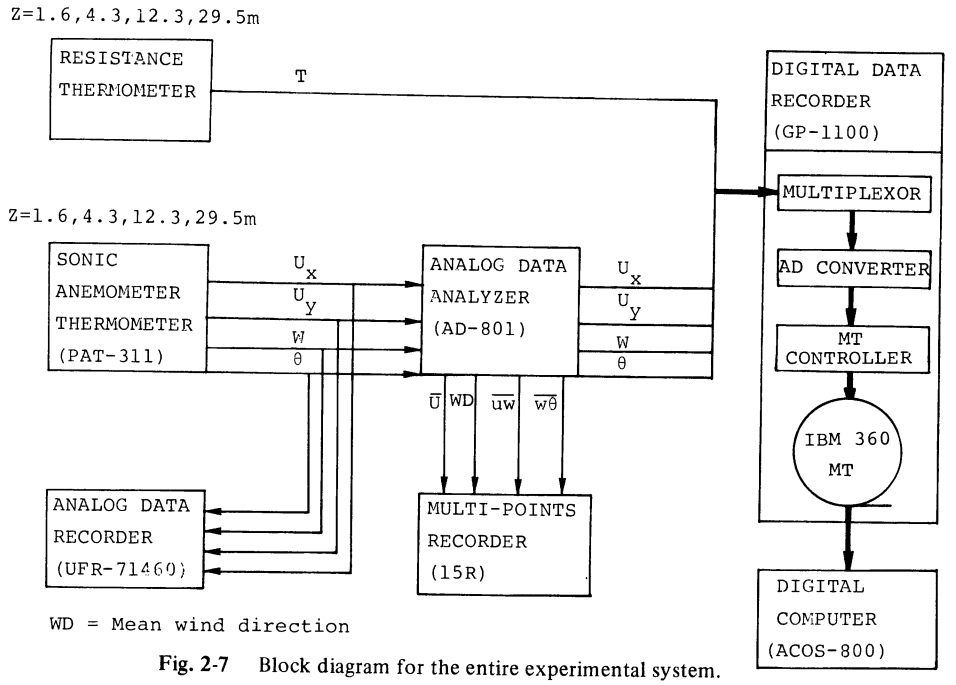

Fig. 2-7 Block diagram for the entire experimental system.

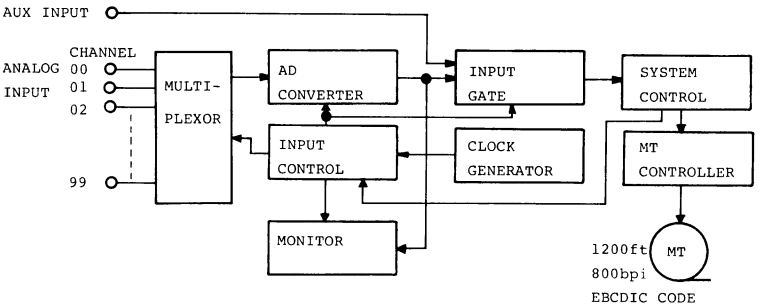

Fig. 2-8 Block diagram of the computer-controlled data acquisition system (GP-1100).

Table 2-1 Selected runs for analysis

Run No.	Date	Starting time	$\bar{U}_{29.5m}$ (m/s)	WD	$\bar{T}_{1.6m}$ (°C)	Stability	Duration (min)
		h m					
230	1/25/79	04 00	0.5		-4.2	Stable	30
240	"	05 00	0.8		-4.4	"	"
250	"	06 00	0.5		-4.8	"	"
260	"	07 00	0.3		-4.6	"	"
270	"	08 00	1.0		-0.2	Neutral	"
280	"	09 00	1.4		4.5	Unstable	"
290	"	10 00	2.2		6.3	"	"
760	7/26/79	11 00	3.5	E	28.1	"	90
770	"	12 40	4.3	E	29.8	"	"
780	"	14 20	5.3	E	29.2	Neutral	"
790	"	23 02	2.1	E	23.1	Stable	"
830	7/29/79	22 20	2.4	ESE	24.1	"	"
980	8/1/79	14 00	5.0	SSW	31.2	Neutral	"

temperature signals in order to reduce the effect of ultra-low-frequency fluctuations. Unless otherwise noted, the results to be presented will be based on the basic 30 min-averaged data which is the average of three consecutive 10 min-averaged groups of data.

Analog signals from the sonic anemometer-thermometers were sampled 20 times a second, digitized and stored on magnetic tapes by means of the 100-channel data acquisition system. The data were filtered with a band-pass digital filter with a frequency range from 0.0024 to 10 Hz in order to give good spectral resolution and to minimize the effect of aliasing.

Data reduction was performed on an ACOS-800 computer, using the statistical and spectral programs developed for this study.

The signals from the sonic anemometer-thermometers were combined to produce the mean wind speed, fluctuations in the three orthogonal components and fluctuations of temperature. The longitudinal and lateral velocity components were transformed to make them correspond to the conventional meteorological coordinate system. The x axis, which defines the u component, is in the direction of the mean wind; the z axis, which defines the w component, is in the vertical direction; the y axis, which defines the component, is perpendicular to x and z in a right-handed coordinate system.

Turbulence statistics, such as variances, covariances, triple moments and their gradients were computed directly from the simultaneously-sampled time series of u, v, w and θ, which represent the departures of the longitudinal, lateral and vertical velocity components and temperature from their respective means.

The power spectra of the turbulent velocity and temperature were obtained using the Fast Fourier Technique (Hino, 1977). The resulting spectra were smoothed with a 3-point running average, to cover the 0.01 to 5 Hz. They were used to estimate the dissipation rate.

CHAPTER 3

THEORETICAL RELATIONS AND METHODS OF ANALYSIS

The surface boundary layer is governed by a set of flow parameters. This flow structure is quite similar to that in the turbulent boundary layer along a flat plate in a wind tunnel. This analogy is essential for theoretical studies.

According to flow properties, the vertical structure of the atmosphere may be classified into three layers as shown in Fig. 3-1. The free atmosphere is free from the influence of surface friction on air motion, and its motion is treated as laminar flow. The planetary boundary layer, in which the influence of surface friction is appreciable, is analogous to the turbulent boundary layer found on a flat plate, and its motion is treated as turbulent flow. The surface boundary layer is the lowest thirty meters, or so, of the planetary boundary layer, where the motion is controlled predominantly by the presence of surface friction. This layer is also referred as the "constant flux layer", where the vertical fluxes of physical properties by turbulence, such as the Reynolds stress and sensible heat flux, are assumed to be constant to a good approximation.

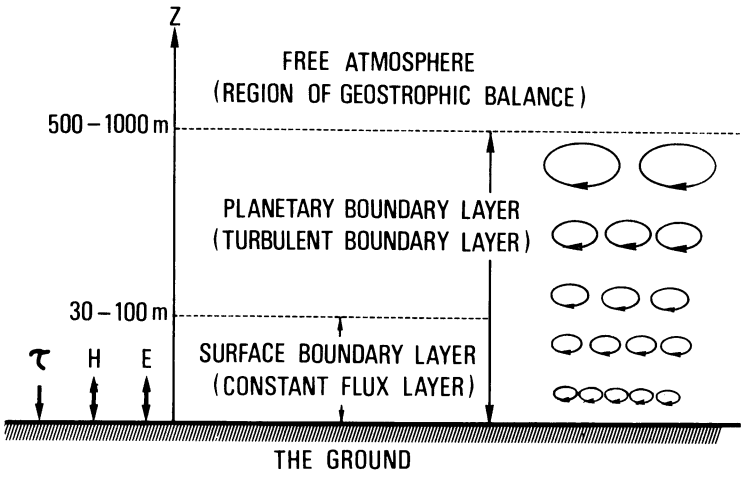

Fig. 3-1 Vertical structure of the atmosphere.

Basic equations and the methods of obtaining the model of the turbulent energy budget will be outlined in this chapter, including the Navier-Stokes equations for laminar flow, the Reynolds equations for turbulent flow, the equation for the constant flux layer, the equation for the turbulent energy budget, the flux-profile relationships, Kolmogorov's $-5/3$ power law, the Monin-Obukhov similarity theory, etc. The relations among the basic equations are schematically given in Fig. 3-2.

3-1 Theoretical relations

a) Equations of motion in the surface boundary layer

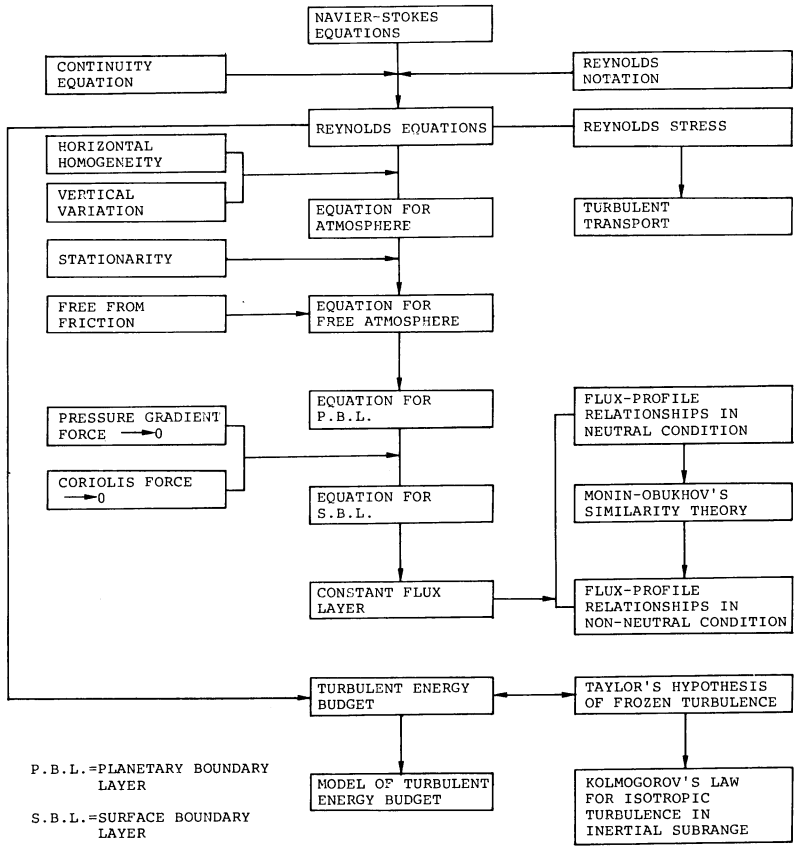

Fig. 3-2 Relation of the equations used in the present study.

The structure of the surface boundary layer will first be explained with the aid of the fundamental principle governing the motion of the atmosphere near the surface of the ground.

This principle is expressed by the Navier-Stokes equations for a viscous, incompressible, Newtonian medium in a uniform gravitational field, in a rotating system, which may be written in the form

$$\begin{aligned}
&\frac{\partial U}{\partial t} + U\frac{\partial U}{\partial x} + V\frac{\partial U}{\partial y} + W\frac{\partial U}{\partial z} = -\frac{1}{\rho}\frac{\partial P}{\partial x} + \nu\nabla^2 U + fV \\
&\frac{\partial V}{\partial t} + U\frac{\partial V}{\partial x} + V\frac{\partial V}{\partial y} + W\frac{\partial V}{\partial z} = -\frac{1}{\rho}\frac{\partial P}{\partial y} + \nu\nabla^2 V - fU \qquad \cdots\cdots\cdots (3\text{-}1) \\
&\frac{\partial W}{\partial t} + U\frac{\partial W}{\partial x} + V\frac{\partial W}{\partial y} + W\frac{\partial W}{\partial z} = -\frac{1}{\rho}\frac{\partial P}{\partial z} + \nu\nabla^2 W - g
\end{aligned}$$

where (U, V, W) are the velocity components of the instantaneous wind vector, f is the Coriolis parameter, (x, y, z) represent the Cartesian coordinate system, P is the pressure, ρ is the air density, g is the acceleration due to gravity, ν is the kinematic viscosity and ∇^2 is Laplacian operator. The first, second and third terms on the right-hand side express the pressure gradient

forces, the friction, and the Coriolis forces or the acceleration due to gravity, respectively.

Eqs. (3-1) represents the instantaneous motion of the atmosphere. It is convenient to describe the mean motion of the atmosphere rather than the instantaneous one for turbulent flows. In the following paragraphs, the mean forms of Eqs. (3-1) are shown.

The instantaneous velocity components and pressure may be expressed as the sum of mean and the fluctuation from the mean:

$$\begin{aligned} U &= \overline{U} + u \\ V &= \overline{V} + v \\ W &= \overline{W} + w \\ P &= \overline{P} + p \end{aligned} \quad \cdots\cdots\cdots\cdots\cdots\cdots\cdots\cdots\cdots\cdots\cdots\cdots\cdots\cdots\cdots\cdots\cdots\cdots \quad (3\text{-}2)$$

where the overbar indicates a time mean, $(\overline{U}, \overline{V}, \overline{W})$ are the components of the mean wind vector, $\overline{P}$ is the mean pressure, (u, v, w) are the components of the turbulent wind vector and P is the fluctuating pressure.

By substituting Eqs. (3-2) into Eqs. (3-1) and averaging, we obtain

$$\begin{aligned} &\frac{\partial \overline{U}}{\partial t} + \overline{U}\frac{\partial \overline{U}}{\partial x} + \overline{V}\frac{\partial \overline{U}}{\partial y} + \overline{W}\frac{\partial \overline{U}}{\partial z} + \frac{\partial}{\partial x}\overline{uu} + \frac{\partial}{\partial y}\overline{uv} + \frac{\partial}{\partial z}\overline{uw} = -\frac{1}{\rho}\frac{\partial \overline{P}}{\partial x} + \nu\nabla^2\overline{U} + f\overline{V} \\ &\frac{\partial \overline{V}}{\partial t} + \overline{U}\frac{\partial \overline{V}}{\partial x} + \overline{V}\frac{\partial \overline{V}}{\partial y} + \overline{W}\frac{\partial \overline{V}}{\partial z} + \frac{\partial}{\partial x}\overline{vu} + \frac{\partial}{\partial y}\overline{vv} + \frac{\partial}{\partial z}\overline{vw} = -\frac{1}{\rho}\frac{\partial \overline{P}}{\partial y} + \nu\nabla^2\overline{V} - f\overline{U} \\ &\frac{\partial \overline{W}}{\partial t} + \overline{U}\frac{\partial \overline{W}}{\partial x} + \overline{V}\frac{\partial \overline{W}}{\partial y} + \overline{W}\frac{\partial \overline{W}}{\partial z} + \frac{\partial}{\partial x}\overline{wu} + \frac{\partial}{\partial y}\overline{wv} + \frac{\partial}{\partial z}\overline{ww} = -\frac{1}{\rho}\frac{\partial \overline{P}}{\partial z} + \nu\nabla^2\overline{W} - g \end{aligned}$$

$$\cdots\cdots\cdots\cdots\cdots\cdots\cdots\cdots\cdots\cdots\cdots\cdots\cdots\cdots\cdots\cdots\cdots\cdots \quad (3\text{-}3)$$

In arriving at Eqs. (3-3), use has also been made of the equation of continuity:

$$\frac{\partial U}{\partial x} + \frac{\partial V}{\partial y} + \frac{\partial W}{\partial z} = 0 \quad \cdots\cdots\cdots\cdots\cdots\cdots\cdots\cdots\cdots\cdots\cdots\cdots\cdots\cdots\cdots\cdots\cdots\cdots \quad (3\text{-}4)$$

Eqs. (3-3) are referred to as the Reynolds equations. Each equation in Eqs. (3-3) has the same form as Eqs. (3-1), except that certain additional terms depending on the fluctuations, viz.,

$$-\rho\overline{uu}, -\rho\overline{vv}, -\rho\overline{ww}, -\rho\overline{uv}, -\rho\overline{uw}, -\rho\overline{vw} \quad \cdots\cdots\cdots\cdots\cdots\cdots\cdots\cdots\cdots\cdots\cdots\cdots\cdots\cdots\cdots\cdots\cdots\cdots \quad (3\text{-}5)$$

have been added. These terms, called the Reynolds stress, indicate that velocity fluctuations, like the molecular process, cause transport of momentum across a surface in the atmosphere. In general, the Reynolds stress outweighs in importance the purely viscous stress, which often may be neglected in problems of turbulent motion. The bar above each term of Eq. (3-5) indicates an integral mean, which may be approximated by the arithmetric mean of the form

$$-\rho\overline{uw} = -\rho(u_1 w_1 + u_2 w_2 + \ldots + u_N w_N)/N \quad \cdots\cdots\cdots\cdots\cdots\cdots\cdots\cdots\cdots\cdots\cdots\cdots\cdots\cdots\cdots\cdots\cdots\cdots \quad (3\text{-}6)$$

Within the planetary boundary layer the vertical variation is usually considerable greater than the horizontal variations, and the fields of meteorological variables are approximately horizontally homogeneous. Taking these assumptions together with the stationary conditions, the following equations in the planetary boundary layer are obtained:

$$0 = -\frac{1}{\rho}\frac{\partial \bar{P}}{\partial x} + \frac{\partial}{\partial z}(-\rho\overline{uw}) + f\bar{V}$$
$$0 = -\frac{1}{\rho}\frac{\partial \bar{P}}{\partial y} + \frac{\partial}{\partial z}(-\rho\overline{vw}) - f\bar{U} \quad \ldots\ldots (3\text{-}7)$$

By analogy to the molecular stress, the Reynolds stress is written as follows:

$$\tau = -\rho\overline{uw} = \rho K_m \frac{\partial \bar{U}}{\partial z} \quad \ldots\ldots (3\text{-}8)$$

where τ is the Reynolds stress and K_m is the turbulent diffusivity of momentum. Eq. (3-8) means that the Reynolds stress is a measure of the vertical transport of momentum. Similarly, the vertical transport of sensible heat may be estimated by an analogous equation;

$$H = \rho c_p \overline{w\theta} = \rho c_p K_h \frac{\partial \bar{T}}{\partial z} \quad \ldots\ldots (3\text{-}9)$$

where H is the sensible heat flux, K_h is the turbulent diffusivity of sensible heat and θ is the fluctuating temperature.

The surface boundary layer is the shallow layer immediately adjacent to the ground in which the frictional drag force τ is the dominant force on the layer. Fig. 3-1 schematically shows this layer, together with the planetary boundary layer and the free atmosphere. To a good approximation, the equation of motion in the surface boundary layer is derived by neglecting the pressure gradient term and the Coriolis force term in Eqs. (3-7):

$$\frac{\partial}{\partial z}(-\rho\overline{uw}) = 0 \quad \ldots\ldots (3\text{-}10)$$

Rewriting the above equation,

$$\tau = -\rho\overline{uw} = \rho K_m \frac{\partial \bar{U}}{\partial z} = \text{constant}\ (z) \quad \ldots\ldots (3\text{-}11)$$

This means that the surface boundary layer is characterized essentially by the "constant flux layer".

b) The structure of the surface boundary layer

The wind profile in the absence of buoyancy is given by:

$$\frac{\partial \bar{U}}{\partial z} = \frac{u_*}{kz} \quad \ldots\ldots (3\text{-}12)$$

where k is the Kármán constant and u_* is the friction velocity, which is defined by the equation

$$u_* = \sqrt{\tau/\rho} = \sqrt{-\overline{uw}} \quad \ldots\ldots (3\text{-}13)$$

u_* is employed as the reference velocity in the study of fluid flow over a rough surface, and generally increases with the mean wind speed and with the roughness of the surface (z_0). Integration of Eq. (3-12) leads to:

$$\bar{U} = \frac{u_*}{k} \ln \frac{z}{z_0} \quad \ldots\ldots (3\text{-}14)$$

where z_0 is the height above the ground where the velocity of air vanishes and is known as the roughness length, a characteristic of the surface.

Monin and Obukhov (1954) modified Eq. (3-12) for use under all stability conditions by

$$\frac{\partial \bar{U}}{\partial z} = \frac{u_*}{kz}\phi_M(z/L) \quad \cdots\cdots (3\text{-}15)$$

where ϕ_M (z/L) is a universal function of z/L, and L (the Monin-Obukhov stability length) is given by

$$L = -\frac{u_*^3 \rho c_p \bar{T}}{kgH} \quad \cdots\cdots (3\text{-}16)$$

With the upward heat flux taken as positive, L is negative. In terms of Eq. (3-15), ϕ_M (z/L) has been set equal to unity in neutral conditions $(z/L = 0)$.

Another important parameter of atmospheric stability, the Richardson number, designated R_i and defined as the non-dimensional quantity

$$R_i = \frac{\frac{g}{\bar{T}}(\frac{\partial \bar{T}}{\partial z})}{(\frac{\partial \bar{U}}{\partial z})^2} \quad \cdots\cdots (3\text{-}17)$$

where g is the gravitational acceleration, and $\partial T/\partial z$ and $\partial U/\partial z$ are the gradients of mean temperature and wind speed, respectively.

An equivalent "flux form" of the parameter is

$$R_f = \frac{g}{\bar{T}} \frac{\overline{w\theta}}{\overline{uw}\frac{\partial \bar{U}}{\partial z}} = \frac{gH}{c_p \bar{T}\tau(\frac{\partial \bar{U}}{\partial z})} \quad \cdots\cdots (3\text{-}18)$$

where R_f is the flux Richardson number, H is the vertical flux of sensible heat and τ the Reynolds stress.

The sign of R_i is determined by the gradient of mean temperature which is, by convention, negative in lapse and positive in inversion profiles. A R_i of zero indicates neutral conditions, negative R_i unstable conditions, and positive R_i stable conditions.

The three stability parameters are related as follows:

$$R_f = \frac{K_h}{K_m} R_i = \frac{z}{L\phi_M} \quad \cdots\cdots (3\text{-}19)$$

Of these parameters z/L is now widely preferred as the most basic for the surface boundary layer, L being independent of height, whereas generally R_i and R_f vary with height, in non-linear way.

According to the Monin-Obukhov similarity theory, the standard deviation, a measure of intensity of turbulence, may be expressed as follows:

$$\frac{\sigma_i}{u_*} = F_i(z/L),\ i = u, v, w \quad \cdots\cdots (3\text{-}20)$$

where σ_i is the standard deviation of the velocity component and F_i (z/L) is the universal function of z/L.

Taylor's hypothesis of frozen turbulence derives the following relation

$$\kappa = 2\pi n/\bar{U} \quad \ldots\ldots\ldots\ldots\ldots\ldots\ldots\ldots\ldots\ldots \quad (3\text{-}21)$$

where κ is the wavenumber and n is the frequency.

Kolmogorov stated that "isotropy of turbulence" stands for the high-frequency region of turbulent fluctuations, where spectra of turbulence follow the -5/3 power law. Detailed treatments of them will be given in the following section.

3-2 Surface-layer similarity

Some of the results will be presented in dimensionless form, and it is appropriate to review the basis for the surface-layer similarity theory.

Dimensional analysis is based on the fact that the fundamental physical laws are dimensionally homogeneous (in mass, length and time, or their combinations), and is used to obtain partial information about the nature of the relation existing among any given set of physical variables.

Similarity theory is a dimensional approach in which characteristic scales of velocity, length, etc., are formed from the physical quantities which are reasoned to determine the properties of flow. Vertical gradients of mean quantities (wind, temperature, etc.) and statistical properties of turbulence (variances, spectra, etc.) are then expressed in dimensionally appropriate combinations of these scales and universal functions of nondimensional parameters.

Similarity theory is essentially a restatement of the cause and effect relation; the result must always be tested experimentally. If conditions surrounding two experiments are identical, the results should be similar. In many micrometeorological cases, however, very little control over experimental conditions is possible. Fortunately, it is not necessary to keep all the variables constant at two sites or at the same site on two different occasions. Complete similarity is achieved if any independent set of dimensionless products of the variables remains constant. For example, a number of pipes with different diameters have similar flows if the Reynolds numbers are all the same.

Dimensional analysis and similarity theory are extensively used in micrometeorology. It is no exaggeration to state that practically the whole theory of the surface boundary layer is derived from these two fundamental principles (Munn, 1966).

One of the most successful tools in the analysis of turbulence in the surface boundary layer has been the Monin-Obukhov similarity theory. This similarity theory has been widely used as a basis for the description of mean wind and temperature as a function of height in the surface boundary layer, defined as the layer near the earth's surface in which the turbulent fluxes are approximately constant with height. The similarity theory suggested that the average wind and temperature fields of the surface boundary layer should depend only on the sensible heat flux H, height from the ground z, the buoyancy parameter $g/\bar{T}$, and the Reynolds stress τ. These define the following velocity, temperature and length scales:

$$\begin{aligned} u_* &= \sqrt{(\tau/\rho)} \\ T_* &= -H/(\rho c_p u_*) \\ z \text{ and } L &= -\frac{u_*^3 \rho c_p \bar{T}}{kgH} \end{aligned} \quad \ldots\ldots\ldots\ldots\ldots\ldots\ldots\ldots \quad (3\text{-}22)$$

Therefore, the four governing surface-layer parameters (H, z, $g/\overline{T}$, τ) yield a total of four independent velocity, temperature and length scales. It is customary to use one velocity scale (u_*), one temperature scale (T_*) and two length scales (z and L). Dimensional analysis then predicts that flow properties, after nondimensionalization with these scales, are functions only of z/L. The terms in the budget equation of turbulent energy (1-1), when nondimensionalized, appear to be functions only of z/L.

The results have been analyzed in dimensionless form, using the following dimensionless quantities:

z/L	Monin-Obukhov stability parameter
$\phi_\epsilon(z/L) = \frac{kz}{u_*^3}\epsilon$	dimensionless viscous dissipation of turbulent energy
$\phi_M(z/L) = \frac{kz}{u_*}\frac{\partial \overline{U}}{\partial z}$	dimensionless term of mechanical production of turbulent energy
$\phi_B(z/L) = \frac{kz}{u_*^3}\frac{g}{\overline{T}}\overline{w\theta}$	dimensionless term of buoyant production of turbulent energy
$\phi_T(z/L) = \frac{kz}{u_*^3}\frac{\partial}{\partial z}\frac{\overline{wq^2}}{2}$	dimensionless term of turbulent transport of turbulent energy
$\phi_I(z/L) = \frac{kz}{u_*^3}I$	dimensionless term of the imbalance

3-3 Turbulent energy budget

In this study it is possible to determine all terms in Eq. (1-1) except the pressure transport, which is too difficult to measure. The assumptions of horizontal homogeneity and stationarity are primarily responsible for the simplification of Eq. (1-1) for the turbulent energy budget. The assumption of stationarity leads to:

$$\frac{\partial}{\partial t}\frac{\overline{q^2}}{2} = 0 \qquad \text{(3-24)}$$

It seems preferable to lump possible inhomogeneity effects together with the pressure transport, and call this the imbalance term IM. For our idealized conditions, we therefore take as our model of the turbulent energy budget

$$-\overline{uw}\frac{\partial \overline{U}}{\partial z} + \frac{g}{\overline{T}}\overline{w\theta} - \frac{\partial}{\partial z}\frac{\overline{wq^2}}{2} - \epsilon + I = 0 \qquad \text{(3-25)}$$

(MP) (BP) (TT) (VD) (IM)

The terms in Eq. (3-25) can be identified as (from the left) mechanical production, buoyant production, turbulent transport, viscous dissipation and the imbalance.

In the surface boundary layer, Eq. (3-25) may conveniently be expressed in dimensionless form, by multiplying through by kz/u_*^3, where $u_* = (\sqrt{\tau/\rho}) = (\sqrt{-\overline{uw}})$ and k is Kármán constant,

$$\frac{kz}{u_*}\frac{\partial \bar{U}}{\partial z} + \frac{kz}{u_*^3}\frac{g}{\bar{T}}\overline{w\theta} - \frac{kz}{u_*^3}\frac{\partial}{\partial z}\frac{\overline{wq^2}}{2} - \frac{kz}{u_*^3}\epsilon + \frac{kz}{u_*^3}I = 0$$

or

$$\phi_M(z/L) - z/L - \phi_T(z/L) - \phi_\epsilon(z/L) + \phi_I(z/L) = 0 \quad \ldots\ldots (3\text{-}26)$$

It has been assumed that the surface layer is a "constant flux layer". That is, the turbulent fluxes $\overline{uw}$ and $\overline{w\theta}$ are approximately independent of height from the surface. For these conditions, the Monin-Obukhov similarity theory predicts that the terms in the budget should be universal function of z/L, which will be determined experimentally and tested in the following chapter.

3-4 Determination of viscous dissipation

Turbulence spectra computed from the measurements are used to estimate viscous dissipation by Kolmogorov's hypothesis on the spectra in the inertial subrange.

Some information about the shape of the spectrum is given by Kolmogorov's hypothesis; energy enters the spectrum at relatively low frequencies and is transferred to higher frequencies until it is finally dissipated. This is called a cascade. All turbulent motions possess local isotropy in the high frequency end of the spectrum. In the local isotropy region, the spectrum of the turbulence, $S(\kappa)$ is determined by viscosity ν and viscous dissipation ϵ. Dimensional arguments leads to

$$S(\kappa) = \epsilon^{2/3}\kappa^{-5/3}G(\kappa, \nu) \quad \ldots\ldots (3\text{-}27)$$

where $G(\kappa, \nu)$ is an undetermined dimensionless function. At the low frequency end of the local isotropic range, viscosity has little effect on $S(\kappa)$. This region is called the inertial subrange and in it, $G(\kappa, \nu)$ is constant.

Hence,

$$S(\kappa) = A\epsilon^{2/3}\kappa^{-5/3} \quad \ldots\ldots (3\text{-}28)$$

where A is a universal constant. Schematic representation of energy spectrum of turbulence is given by Fig. 3-3.

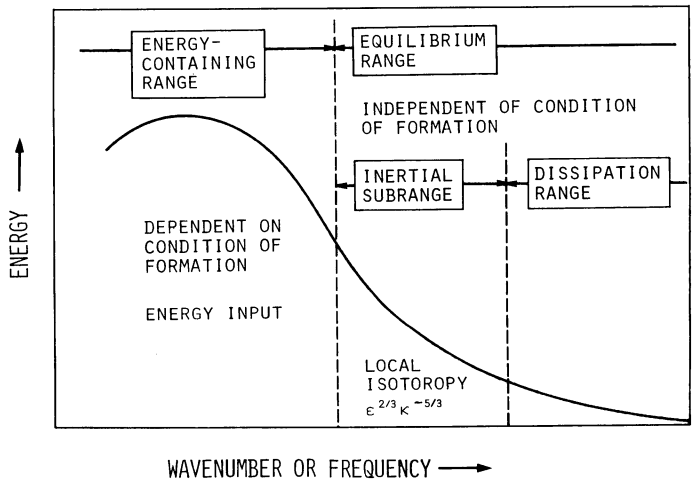

Fig. 3-3 Schematic representation of the energy spectrum of turbulence (from Hinze, 1959).

The estimates of viscous dissipation were obtained by assuming that Kolmogorov's law for the inertial subrange was valid, *i.e.*,

$$\epsilon = \frac{S_i(\kappa)\kappa^{5/3}}{A_i}^{3/2}, \quad i = u, v, w \qquad \text{(3-29)}$$

where κ is the wavenumber ($\kappa = 2\pi n/\bar{U}$ by Taylor's hypothesis). The $-5/3$ power law was fitted to the spectra of velocity components and ϵ was evaluated with $A_u = 0.50$ and $A_v = A_w = 0.67$, which were universal constants estimated from various experiments (Pond et al., 1966; McBean et al., 1971; Wyngaard and Coté 1971).

CHAPTER 4

RESULTS AND DISCUSSION

Section 4-1 describes statistical characteristics of turbulence. Turbulence statistics are analyzed and interpreted in relation to measured parameters, such as height, mean wind speed and stability conditions. Terms in the budget equation of turbulent energy were derived from turbulence statistics, and their behaviors are examined in Section 4-2. The model of the turbulent energy budget is presented and discussed.

Table 4-1 Turbulence statistics (with respect to the 90-min mean) at the four levels of the tower. Each run is classified into three stability groups according to z/L.

Run No.	z (m)	760	770	Mean	780	980	Mean	790	830	Mean
z/L	1.6	−0.12	−0.12	−0.12	−0.05	−0.04	−0.04	0.15	0.18	0.16
	4.3	−0.16	−0.22	−0.19	−0.05	−0.05	−0.05	0.17	0.34	0.26
	12.3	−0.18	−0.20	−0.19	−0.03	−0.08	−0.05	0.09	0.68	0.39
	29.5	−0.27	−0.25	−0.26	−0.07	−0.07	−0.07	1.03	3.21	2.12
$\overline{U}$ (m/s)	1.6	2.20	2.53	2.37	2.86	2.95	2.91	1.07	1.18	1.13
	4.3	2.49	2.90	2.70	3.32	3.49	3.41	1.14	1.29	1.22
	12.3	2.96	3.42	3.19	3.99	4.27	4.13	1.55	1.79	1.67
	29.5	3.51	4.37	3.94	5.30	5.04	5.17	2.13	2.42	2.28
$\overline{T}$ (°C)	1.6	28.1	29.8	29.0	29.1	31.2	30.2	23.1	24.1	23.6
u_* (m/s)	1.6	0.22	0.26	0.24	0.29	0.30	0.29	0.09	0.11	0.10
	4.3	0.28	0.32	0.30	0.38	0.42	0.40	0.12	0.14	0.13
	12.3	0.36	0.47	0.42	0.56	0.50	0.53	0.17	0.17	0.17
	29.5	0.32	0.40	0.36	0.41	0.56	0.49	0.15	0.14	0.15
$\overline{q^2}/2$ (m^2/s^2)	1.6	0.54	0.79	0.67	0.89	1.07	0.98	0.09	0.11	0.10
	4.3	0.62	0.92	0.77	1.05	1.24	1.15	0.11	0.14	0.13
	12.3	0.69	1.04	0.87	1.25	1.52	1.39	0.14	0.19	0.17
	29.5	0.70	0.99	0.84	1.07	1.49	1.28	0.14	0.19	0.16
σ_u (m/s)	1.6	0.63	0.76	0.69	0.84	1.01	0.93	0.29	0.31	0.30
	4.3	0.66	0.83	0.75	0.92	1.07	1.00	0.33	0.34	0.34
	12.3	0.72	0.89	0.81	1.00	1.18	1.09	0.34	0.41	0.38
	29.5	0.71	0.85	0.78	0.95	1.17	1.06	0.35	0.39	0.37
σ_v (m/s)	1.6	0.75	0.91	0.83	0.95	0.95	0.95	0.27	0.30	0.29
	4.3	0.76	0.92	0.84	0.95	0.96	0.96	0.27	0.33	0.30
	12.3	0.74	0.92	0.83	0.97	1.02	1.00	0.32	0.36	0.34
	29.5	0.74	0.91	0.83	0.90	0.96	0.93	0.31	0.37	0.34
σ_w (m/s)	1.6	0.32	0.39	0.35	0.41	0.44	0.43	0.15	0.17	0.16
	4.3	0.44	0.52	0.48	0.58	0.62	0.60	0.20	0.23	0.22
	12.3	0.53	0.65	0.59	0.73	0.76	0.75	0.25	0.27	0.26
	29.5	0.53	0.63	0.58	0.65	0.80	0.72	0.24	0.28	0.26
σ_T (°C)	1.6	0.55	0.66	0.60	0.49	0.45	0.47	0.22	0.24	0.23
	4.3	0.41	0.50	0.45	0.40	0.42	0.41	0.19	0.24	0.22
	12.3	0.34	0.42	0.38	0.38	0.42	0.40	0.21	0.26	0.24
	29.5	0.32	0.38	0.35	0.35	0.40	0.38	0.21	0.25	0.23

4-1 Statistical characteristics of turbulence

a) Mean profiles of turbulence statistics and wind direction

Turbulent statistics were measured at the four levels (1.6, 4.3, 12.3, 29.5 m) of the tower. Table 4-1 gives the resulting data with respect to the 90-min mean. Six runs were selected as representative of typical conditions during the experiment; Run 760 and 770, which represent unstable conditions, and Run 780 and 980, which represent almost neutral conditions, and Run 790 and 830, which represent stable conditions.

Fig. 4-1 shows the profiles of mean wind speed, turbulent energy and standard deviation of temperature. Profiles of other statistics will be presented in the following sections. According to the stability parameter z/L, each profile was divided into the following three cases of unstable, neutral and stable conditions. As can be seen in the figure, the mean wind speed increases linearly with the logarithm of height. Turbulent energy increases with height to reach its maximum at 12.3 m. It seems that turbulent energy is closely related to the mean wind speed. Temperature fluctuations decrease with height, and for stable conditions temperature fluctuations are very small, compared with those for unstable conditions. It seems that the effect of stability is clearly reflected in the magnitude of temperature fluctuations.

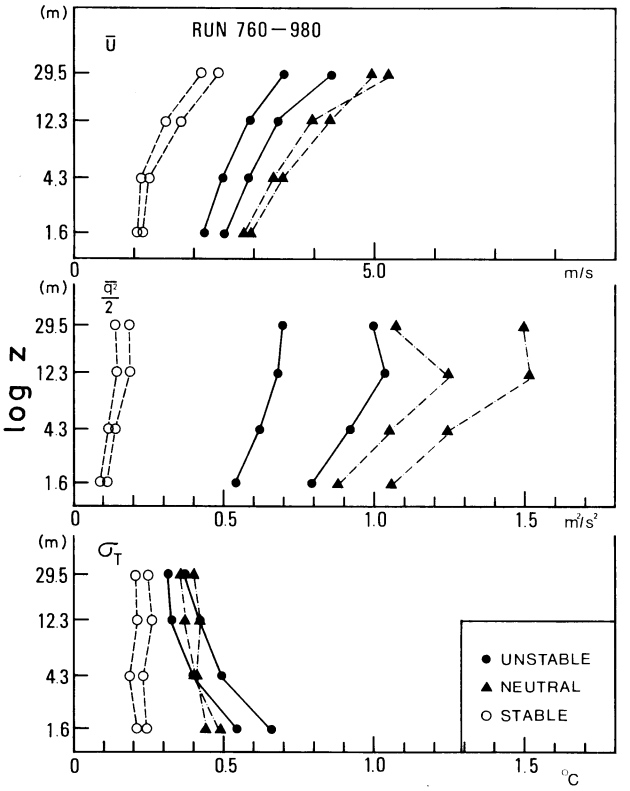

Fig. 4-1 Profiles of mean wind speed, turbulent energy and standard deviation of temperature. Each run is classified into three stability groups according to the stability parameter z/L as follows: ● = unstable conditions, ▲ = neutral conditions, O = stable conditions.

Fig. 4-2 shows wind directions at 1.6 m and 29.5 m during the experiment. Most of the wind directions ranged from the east to south; the data used for analysis are limited to these directions in order to avoid tower influence on wind speed measurements.

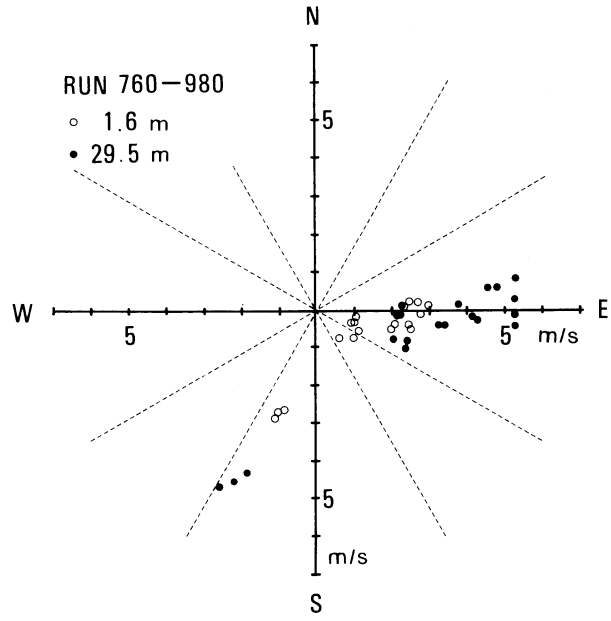

Fig. 4-2 Mean wind directions during the experiment.

b) Friction velocity

The friction velocity u_* is an important parameter of turbulent flow. u_* is introduced into the previously-mentioned similarity theory as the basic velocity scale. The determination of u_* is based on the eddy correlation method given by Eq. (3-8);

$$u_* = \sqrt{\tau/\rho} = \sqrt{-\overline{uw}} \quad \cdots\cdots\cdots\cdots\cdots\cdots\cdots\cdots\cdots\cdots\cdots\cdots \quad (4\text{-}1)$$

The property of $-\overline{uw}$ is related to the gradient of mean wind speed U as follows:

$$u_*^2 = -\overline{uw} = K_m \frac{\partial \overline{U}}{\partial z} \quad \cdots\cdots\cdots\cdots\cdots\cdots\cdots\cdots\cdots\cdots\cdots\cdots \quad (4\text{-}2)$$

where K_m is the turbulent diffusivity for momentum. In order to examine the above relation, the values for u_*^2 at 12.3 m are plotted against the gradients of mean wind speed, $\partial\overline{U}/\partial z$ calculated from the data at 4.3 m and 29.5 m. The result is shown in Fig. 4-3. It appears from the figure that u_*^2 is proportional to the gradient of mean wind speed, and the coefficient K_m is about 4 m^2/s.

Fig. 4-4 shows the friction velocity u_* as a function of mean wind speed $\overline{U}$. These values were evaluated at four levels (1.6, 4.3, 12.3, 29.5 m). As can be seen in the figure, u_* increases linearly with $\overline{U}$ at each level, and this relation between u_* and $\overline{U}$ is consistent with pervious studies. The relation between u_* and $\overline{U}$ at each level is expressed by:

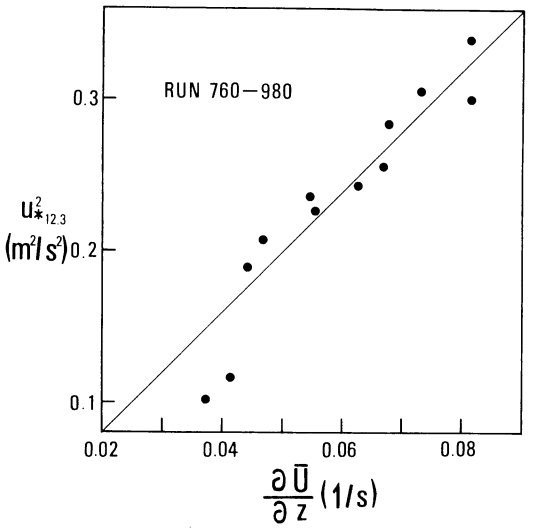

Fig. 4-3 u_*^2 at 12.3 m against the gradient of mean wind speed between 4.3 m and 29.5 m.

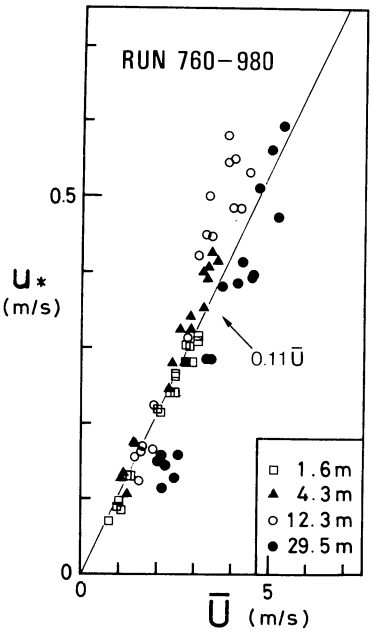

Fig. 4-4 Friction velocity as a function of mean wind speed. Symbols represent different heights as follows: □ = 1.6 m, ▲ = 4.3 m, ○ = 12.3 m, ● = 29.5 m.

$$
\begin{aligned}
u_* &= 0.10\ \bar{U} \text{ at } 1.6 \text{ m} \\
u_* &= 0.12\ \bar{U} \text{ at } 4.3 \text{ m} \\
u_* &= 0.12\ \bar{U} \text{ at } 12.3 \text{ m} \\
u_* &= 0.09\ \bar{U} \text{ at } 29.5 \text{ m} \\
u_* &= 0.11\ \bar{U} \text{ in the whole layer}
\end{aligned}
\qquad \ldots\ldots\ldots\ldots\ldots\ldots\ldots\ldots\ldots\ldots (4\text{-}3)
$$

c) Intensity of turbulence

The standard deviations of the velocity components σ_i (i = u, v, w) represent the magnitude of turbulent fluctuations. Generally speaking, turbulent fluctuations are closely related to the atmospheric stability and the mean wind speed. In this section, these relationships will be examined.

Fig. 4-5 shows records of the instantaneous velocity components (U, W) for unstable and stable conditions. From the figure it is seen that the fluctuations of the longitudinal component U are larger than those of the vertical component W, and the fluctuations of turbulence for stable conditions are considerable smaller as compared with those of the unstable case.

Fig. 4-6 shows profiles of the ratio $\sigma_i/\bar{U}$ (i = u, v, w) classified into three cases of unstable, neutral and stable conditions. The ratio is regarded as the intensity of turbulence. It can be seen from the figure that the ratios for horizontal components, $\sigma_u/\bar{U}$, $\sigma_v/\bar{U}$ decrease with height, but the ratio for the vertical component, $\sigma_w/\bar{U}$ is almost constant with height.

Fig. 4-7 shows the standard deviations of the velocity components σ_i (i = u, v, w) as functions of mean wind speed $\bar{U}$ at the four heights. It may be seen that σ_i (i = u, v, w) increase with $\bar{U}$. It is noticed that the scatter for the vertical component is relatively small as compared with those for the horizontal components. The ratios of $\sigma_i/\bar{U}$ (i = u, v, w) are listed in Table 4-2. The ratio at the

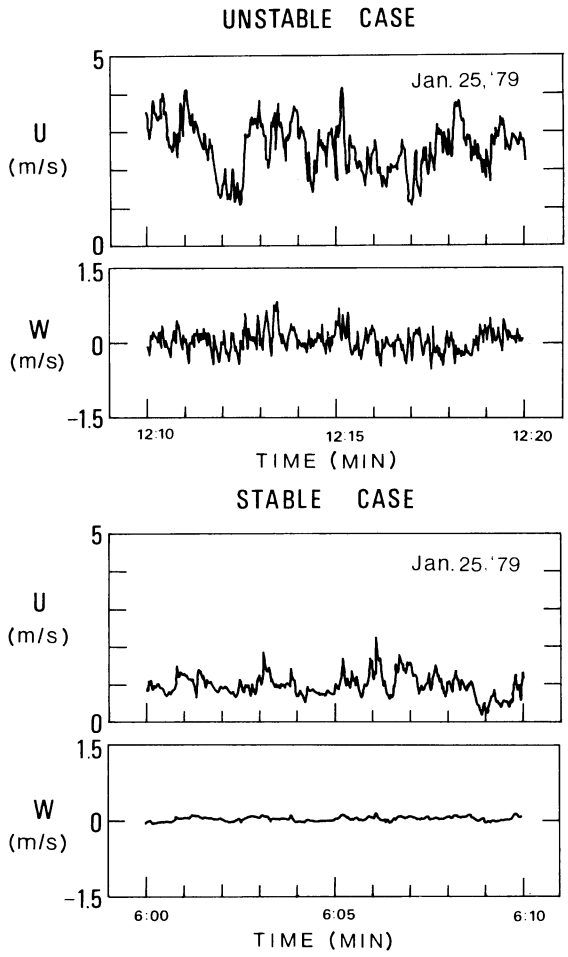

Fig. 4-5 Record of instantaneous velocity components U, W.

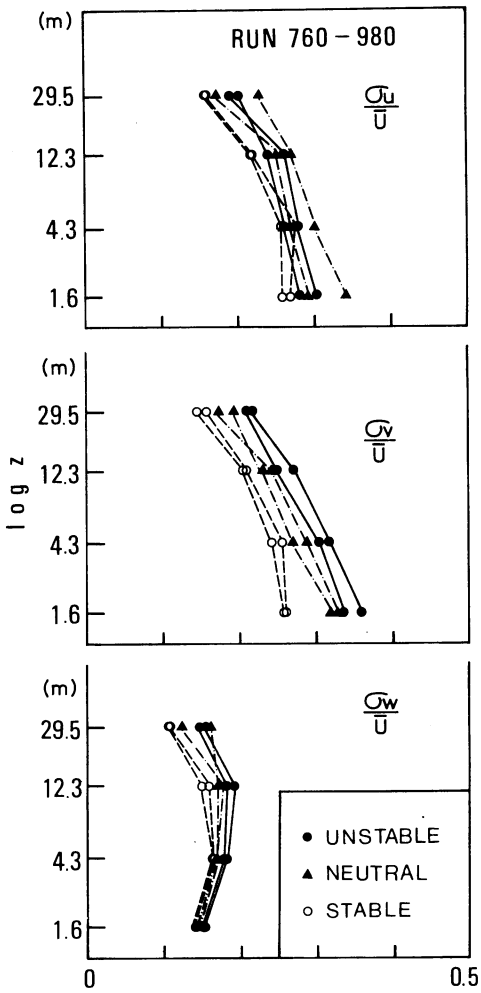

Fig. 4-6 Profiles of the ratios, $\sigma_i/\overline{U}$ (i = u, v, w). Symbols are the same as those in Fig. 4-1.

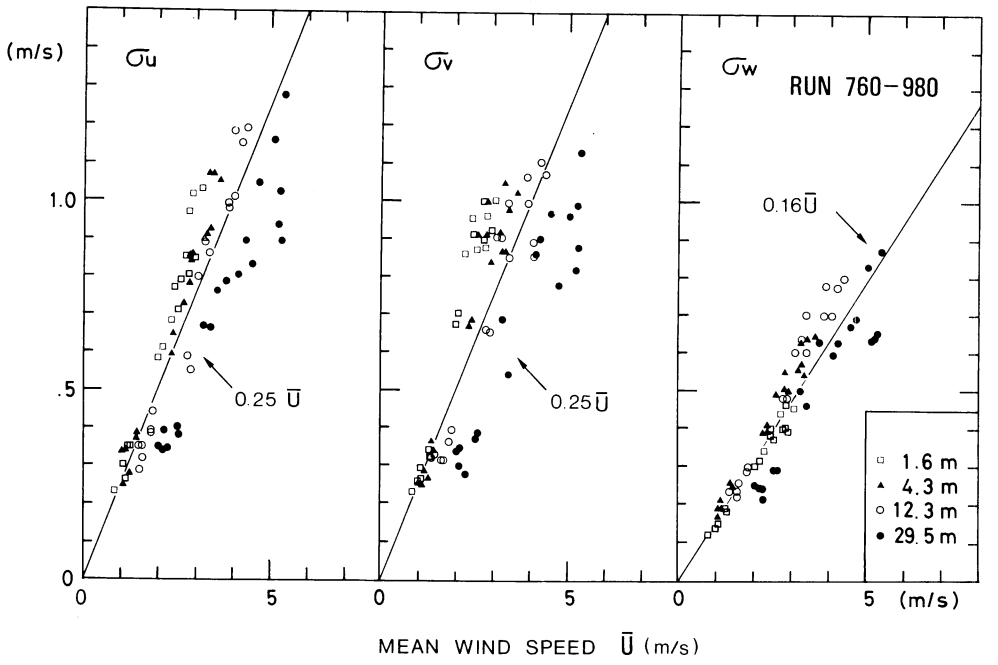

Fig. 4-7 Standard deviations of the velocity components as a function of mean wind speed. Symbols are the same as those in Fig. 4-4.

highest height (z = 29.5 m) is slightly smaller than those at the lower heights (z = 1.6 to 12.3 m). The vertical variation of $\sigma_w/\overline{U}$ is rather small.

Fig. 4-8 shows the standard deviations of the velocity components σ_i (i = u, v, w) as a function of friction velocity u_* at four heights. It may be seen that σ_i (i = u, v, w) increase with the friction velocity u_*. It is noticed that for the cases of the horizontal components there is a great deal of scatter in comparison with the case of the vertical component. The vertical component near the ground does not contain the low frequency components of fluctuations, which are affected by the variation of wind direction and the stability of the atmosphere, and so σ_w has the simple dependence on u_*.

The relations between σ_i (i = u, v, w) and u_* are expressed by

$$\sigma_i = C_i u_*, \quad i = u, v, w \quad \ldots\ldots\ldots\ldots\ldots\ldots\ldots\ldots\ldots\ldots (4\text{-}4)$$

where C_i is the coefficient. The values for C_i are listed in Table 4-2. As can be seen in the table, the ratios vary with height. The ratio of σ_u/u_* at the lower level (1.6 m) is 20% larger than one at the upper level (29.5 m). This trend is recognized for the horizontal components, but not for the vertical component.

The value for σ_w/u_* in neutral conditions is listed in Table 4-3 and is compared with other results. Values obtained in the present study are in agreement with the results by other researchers. Pond et al. (1971) showed the value of 1.32 ± 0.26 over the sea, and McBean (1970) of 1.53 ± 0.16 over land.

The ratio σ_w/u_* may be given by a universal function of the stability parameter z/L according

Table 4-2 Data summary for the ratios of $\sigma_i/\overline{U}$ and σ_i/u_* (i = u, v, w) with respect to the 90-min mean. Each run is classified into three stability groups according to z/L.

Run No.	z (m)	760	770	Mean	780	980	Mean	790	830	Mean
z/L	1.6	−0.12	−0.12	−0.12	−0.05	−0.04	−0.04	0.15	0.18	0.16
	4.3	−0.16	−0.22	−0.19	−0.05	−0.05	−0.05	0.17	0.34	0.26
	12.3	−0.18	−0.20	−0.19	−0.03	−0.08	−0.05	0.09	0.68	0.39
	29.5	−0.27	−0.25	−0.26	−0.07	−0.07	−0.07	1.03	3.21	2.12
$\sigma_u/\overline{U}$	1.6	0.28	0.30	0.29	0.29	0.34	0.32	0.27	0.26	0.27
	4.3	0.27	0.29	0.28	0.28	0.31	0.29	0.29	0.26	0.28
	12.3	0.24	0.26	0.25	0.25	0.28	0.26	0.23	0.23	0.23
	29.5	0.20	0.29	0.20	0.18	0.23	0.21	0.16	0.16	0.16
$\sigma_v/\overline{U}$	1.6	0.34	0.36	0.35	0.33	0.32	0.33	0.26	0.26	0.26
	4.3	0.30	0.32	0.31	0.28	0.28	0.28	0.25	0.26	0.25
	12.3	0.25	0.27	0.26	0.25	0.24	0.24	0.21	0.20	0.21
	29.5	0.21	0.21	0.21	0.17	0.19	0.18	0.15	0.16	0.15
$\sigma_w/\overline{U}$	1.6	0.15	0.15	0.15	0.15	0.15	0.15	0.14	0.14	0.14
	4.3	0.18	0.18	0.18	0.18	0.18	0.18	0.18	0.18	0.18
	12.3	0.18	0.19	0.18	0.18	0.18	0.18	0.16	0.15	0.16
	29.5	0.15	0.15	0.15	0.12	0.16	0.14	0.11	0.11	0.11
σ_u/u_*	1.6	2.77	2.99	2.88	2.90	3.41	3.16	3.15	2.97	3.06
	4.3	2.37	2.74	2.56	2.42	2.60	2.51	2.69	2.54	2.62
	12.3	2.06	1.95	2.01	1.79	2.37	2.08	2.10	2.53	2.32
	29.5	2.29	2.15	2.22	2.37	2.10	2.24	2.31	2.99	2.65
σ_v/u_*	1.6	3.30	3.57	3.44	3.29	3.18	3.24	3.04	2.01	2.98
	4.3	2.72	3.06	2.90	2.51	2.34	2.43	2.33	2.50	2.42
	12.3	2.13	2.09	2.11	1.73	2.06	1.90	1.94	2.28	2.12
	29.5	2.39	2.38	2.39	2.26	1.73	2.00	2.11	2.82	2.47
σ_w/u_*	1.6	1.44	1.50	1.47	1.43	1.49	1.47	1.65	1.57	1.61
	4.3	1.57	1.72	1.65	1.53	1.52	1.53	1.66	1.73	1.70
	12.3	1.50	1.44	1.47	1.31	1.53	1.42	1.52	1.67	1.60
	29.5	1.69	1.64	1.67	1.62	1.44	1.53	1.61	2.06	1.84

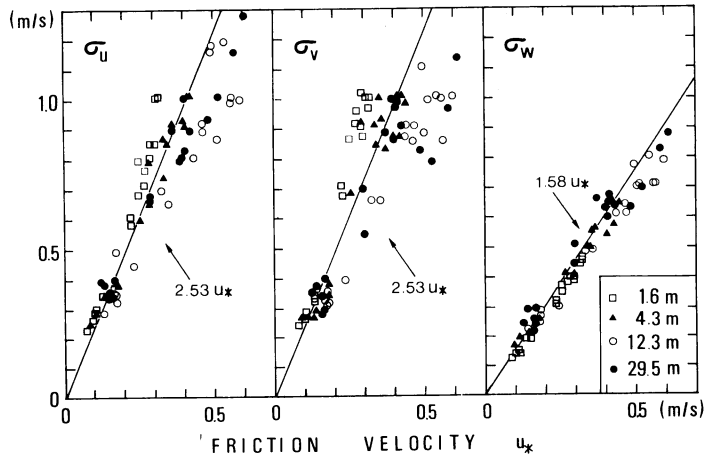

Fig. 4-8 Standard deviations of the velocity components as a function of friction velocity. Symbols are the same as those in Fig. 4-4.

Table 4-3 Comparison of the ratio σ_w/u_* with other results under neutral conditions

Reference for estimate		σ_w/u_*	Site	Height of measurements (m)
Naito	1978	1.23	Over the sea	12.5, 6.4
Pond et al.	1971	1.32	Over the sea	8
Miyake et al.	1970	1.47	Over the sea	1.4 – 4.5
McBean	1970	1.53	Over land	1.4
This study		1.32	Tsukuba	1.6, 4.3, 12.3, 29.5

Estimates are obtained by the eddy correlation method.

to the similarity theory. Fig. 4-9 shows σ_w/u_* versus z/L, in order to clarify the features of the ratios over a wide range of z/L. The data for the vertical component show the dependence on the stability parameter z/L. The behavior of σ_w/u_* on the unstable side is well expressed by the following equation proposed by Panofsky et al. (1977):

$$\sigma_w/u_* = 1.3\,(1 - 3z/L)^{1/3} \quad \ldots\ldots\ldots\ldots\ldots\ldots\ldots\ldots\ldots\ldots \quad (4\text{-}5)$$

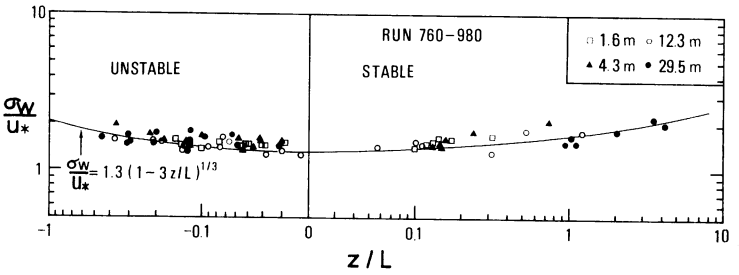

Fig. 4-9 Relationship of the ratio σ_w/u_* to the stability parameter z/L. Symbols are the same as those in Fig. 4-4.

Summarizing the results for turbulence statistics, the following features are shown:

(1) The standard deviations of the velocity components are closely related to mean wind speed, friction velocity and stability. Data for the horizontal components are much more scattered in comparison with those for the vertical component.

(2) The ratio $\sigma_i/\bar{U}$ (i = u, v, w) at the higher levels are rather smaller that those at the lower heights.

(3) The ratio σ_w/u_* depends on stability. Values obtained in the present study agree well with the results by other researchers.

d) Spectra of the velocity components

The spectra were computed using the Fast Fourier Technique. The resulting spectra were obtained by dividing each 90-min record into 9 consecutive 10-min blocks of data and constructing a composite spectrum by averaging the 9 separate spectra. The composite spectrum was then smoothed by averaging spectral estimates over frequency bands. Data for stability and profile are presented in Table 4-1.

The results of this experiment provide an opportunity to examine Kolmogorov's hypothesis for the behavior of the spectra in the inertial subrange. Fig. 4-10 shows the spectra for the longitudinal component u and for the vertical component w at the four levels of the tower, which are

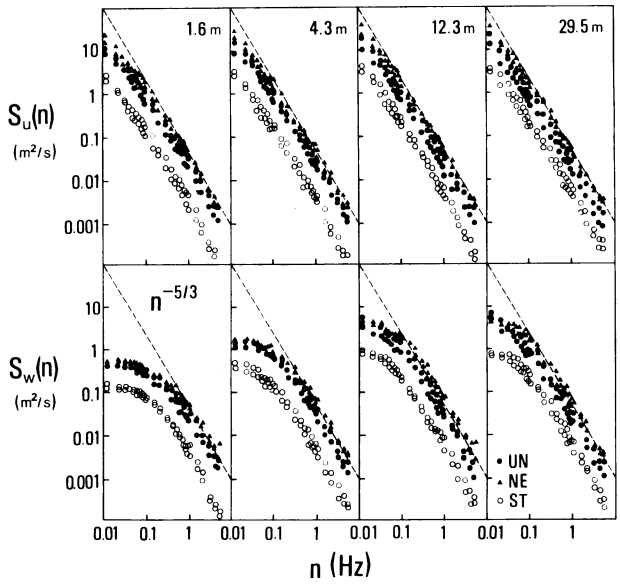

Fig. 4-10 Spectra of the velocity components, $S_i(n)$ (i = u, w) at the four levels of the tower. Symbols are the same as those in Fig. 4-1.

plotted in a log-log representation against frequency n (Hz) and divided into three groups according to the stability parameter z/L indicated in the figure. The broken line in the figure have a slope of −5/3 corresponding to Kolmogorov's hypothesis. Stability effects for the spectra are clearly recognized for unstable and neutral to stable conditions. The spectra of u and w show a well-developed −5/3 slope of inertial subrange on the high-frequency side. The u spectra are found to obey the −5/3 power law at much lower frequencies than the w spectra. The position of the inertial subrange shifts to lower frequencies as increasing height. These results indicate that the horizontal scale of turbulence is larger than the vertical one and that the scale of turbulence increases with height.

The low-frequency limit of the inertial subrange in the atmosphere has been investigated in various ways. On the theoretical side, Hinze (1959) stated that in the inertial subrange the one-dimensional velocity spectra should obey the relation:

$$S_w(n)/S_u(n) = 4/3 \quad \ldots\ldots\ldots\ldots\ldots\ldots\ldots\ldots\ldots\ldots \quad (4\text{-}6)$$

In order to identify the onset of the inertial subrange, the ratio between the spectra of u and w was calculated and shown in Fig. 4-11. It appears that the inertial subrange shifts to lower frequencies as increasing height; for example, the low-frequency limits of the inertial subrange at the levels of 1.6 and 29.5 m are about 1.0 and 0.1 Hz, respectively. The frequency $n_{i.s.}$ at which the inertial subrange starts was evaluated from Fig. 4-11, and the vertical profiles of $n_{i.s.}$ are classified into three stability categories and shown in Fig. 4-12. It can be seen that the inertial subrange shifts to lower frequencies as increasing stability and height.

Fig. 4-13 shows $nS_i(n)$ (i = u, w) plotted against log n. In this figure the area between two frequencies represents variance contributed by that frequency interval, so that

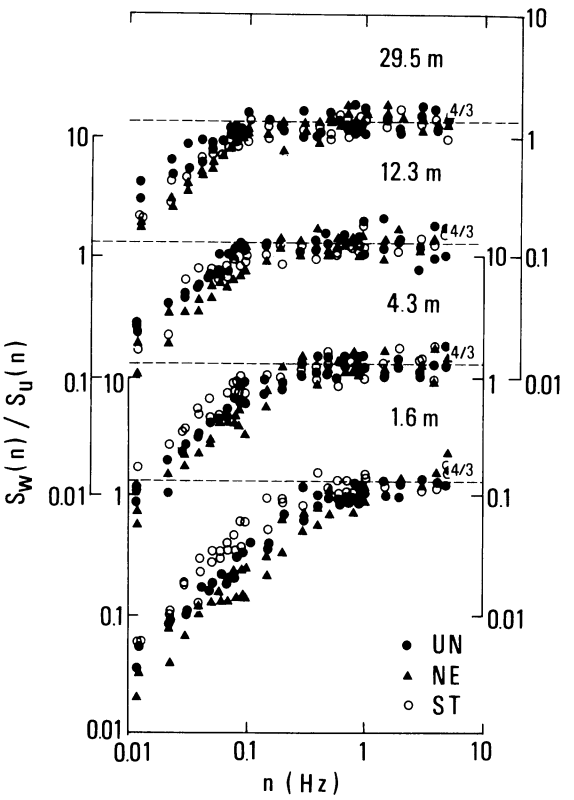

Fig. 4-11 Onset of the 4/3 ratio between the u and w spectra in the inertial subrange. Symbols are the same as those in Fig. 4-1.

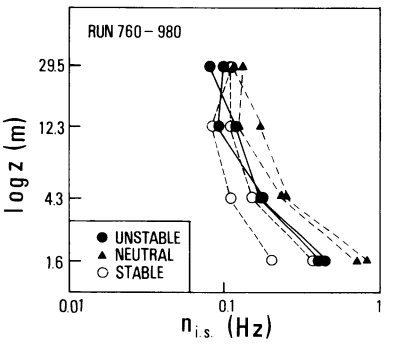

Fig. 4-12 Vertical profiles of the frequency $n_{i.s.}$ which is the lower limit of the inertial subrange. Symbols are the same as those in Fig. 4-1.

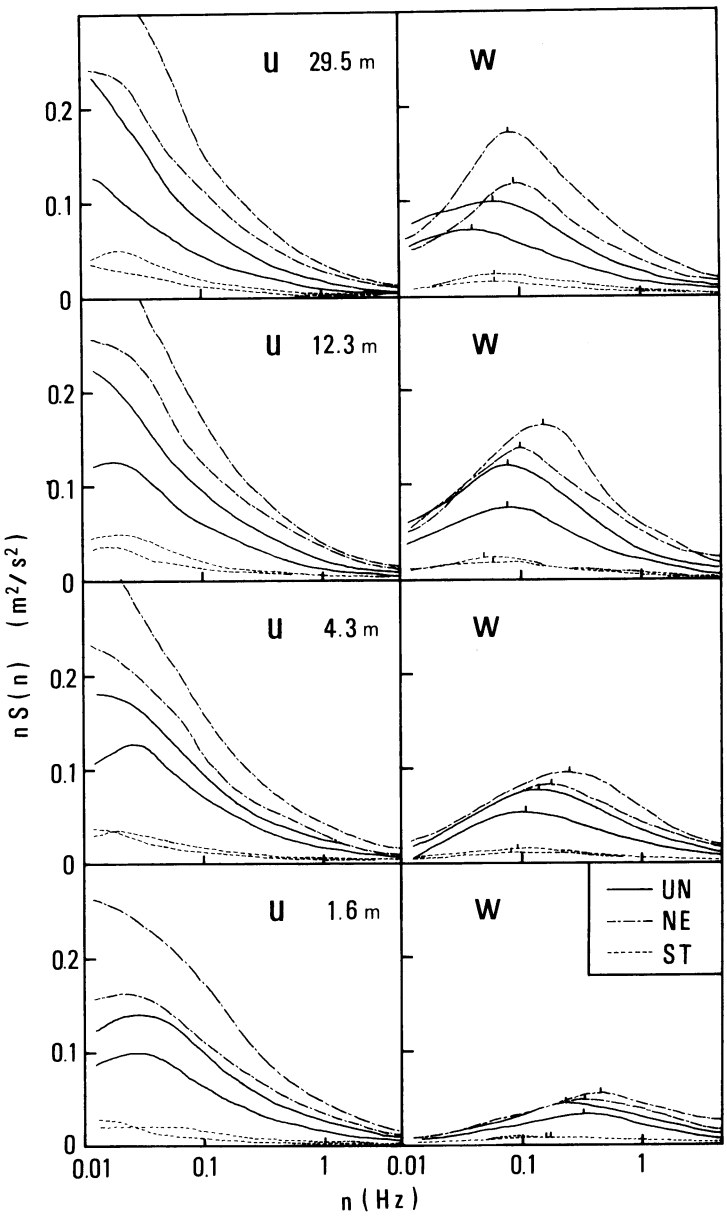

Fig. 4-13 Spectra of the velocity components, $nS_i(n)$ (i = u, w) at the four levels of the tower.

$$\int_0^\infty S_i(n)dn = \int_0^\infty nS_i(n)\, d(\log n) \fallingdotseq \sigma_i^2 \quad \ldots\ldots\ldots\ldots\ldots\ldots \quad (4\text{-}7)$$

where i = u, w. Each curve in the figure is classified into three stability categories. The shape and scale of the spectra will be discussed. As can be seen in the figure, the magnitude of the spectra clearly depends on both stability and mean wind speed; the greater the instability, the more energy is produced. Under all conditions the u spectra contain considerable energy at low frequencies.

The major peak in the spectra is of special interest because the frequency of this peak is generally a good indicator of the characteristic scale of the turbulence. The peak for w as well as u is found to shift systematically to lower frequencies with height. The values of n_m listed in Table 4-4 are from 'eye' estimates of the position of the maximum $nS_w(n)$, and the vertical profiles of n_m are shown in Fig. 4-14. It appears that the vertical profiles of n_m are very similar to those of $n_{i.s.}$. In Fig. 4-15 the peak frequency n_m is plotted against the mean wind speed $\overline{U}$. n_m increases with $\overline{U}$, so that the scale of turbulence decreases with the mean wind speed. The relationships between n_m and $\overline{U}$ at the four levels of the tower are expressed as follows:

$$\begin{aligned} n_m &= 0.13\,\overline{U} + 0.015 \text{ at } 1.6 \text{ m} \\ n_m &= 0.06\,\overline{U} + 0.004 \text{ at } 4.3 \text{ m} \\ n_m &= 0.03\,\overline{U} + 0.002 \text{ at } 12.3 \text{ m} \\ n_m &= 0.01\,\overline{U} + 0.033 \text{ at } 29.5 \text{ m} \end{aligned} \qquad \cdots\cdots\cdots\cdots\cdots\cdots\cdots\cdots (4\text{-}8)$$

There have been several attempts to generalize on the position n_m of the spectral peak (Pasquill,

Table 4-4 Data summary for the spectral scales with respect to the 90-min mean. Each run is classified into three stability groups according to z/L.

Run No.	z (m)	760	770	Mean	780	980	Mean	790	830	Mean
z/L	1.6	−0.12	−0.12	−0.12	−0.05	−0.04	−0.04	0.15	0.18	0.16
	4.3	−0.16	−0.22	−0.19	−0.05	−0.05	−0.05	0.17	0.34	0.26
	12.3	−0.18	−0.20	−0.19	−0.03	−0.08	−0.05	0.09	0.68	0.39
	29.5	−0.27	−0.25	−0.26	−0.07	−0.07	−0.07	1.03	3.21	2.12
$\overline{U}$ (m/s)	1.6	2.20	2.53	2.37	2.86	2.95	2.91	1.07	1.18	1.13
	4.3	2.49	2.90	2.70	3.32	3.49	3.41	1.14	1.29	1.22
	12.3	2.96	3.42	3.19	3.99	4.27	4.13	1.55	1.79	1.67
	29.5	3.51	4.37	3.94	5.30	5.04	5.17	2.13	2.42	2.28
$\overline{T}$ (°C)	1.6	28.1	29.8	29.0	29.1	31.2	30.2	23.1	24.1	23.6
n_m (Hz)	1.6	0.35	0.25	0.30	0.35	0.49	0.42	0.17	0.16	0.17
	4.3	0.10	0.15	0.12	0.18	0.35	0.22	0.08	0.09	0.09
	12.3	0.09	0.08	0.08	0.10	0.16	0.13	0.06	0.05	0.06
	29.5	0.04	0.06	0.05	0.09	0.08	0.85	0.06	0.06	0.06
λ_m (m)	1.6	6.29	10.1	8.20	8.17	6.02	7.10	6.29	7.38	6.84
	4.3	24.9	19.3	22.1	18.4	14.0	16.2	14.3	14.3	14.3
	12.3	32.2	42.8	37.5	39.9	26.7	33.3	25.8	35.8	30.8
	29.5	87.8	72.0	79.9	58.9	63.0	61.0	35.5	40.3	37.9
λ_m/z	1.6	3.93	6.33	5.13	5.11	3.76	4.44	3.93	4.61	4.27
	4.3	5.79	4.50	5.15	4.29	3.25	3.77	3.31	3.33	3.32
	12.3	2.67	3.48	3.08	3.24	2.17	2.71	2.10	2.91	2.51
	29.5	2.97	2.44	2.71	2.00	2.14	2.07	1.20	1.37	1.29
f_m	1.6	0.26	0.16	0.21	0.20	0.27	0.23	0.25	0.22	0.24
	4.3	0.17	0.22	0.20	0.23	0.31	0.27	0.30	0.30	0.30
	12.3	0.37	0.29	0.33	0.31	0.46	0.39	0.48	0.34	0.41
	29.5	0.34	0.23	0.28	0.50	0.47	0.48	0.83	0.73	0.78
$n_{i.s.}$ (Hz)	1.6	0.50	0.55	0.53	0.70	0.83	0.77	0.20	0.37	0.29
	4.3	0.17	0.17	0.17	0.23	0.24	0.24	0.11	0.15	0.13
	12.3	0.12	0.09	0.11	0.12	0.17	0.15	0.09	0.11	0.10
	29.5	0.08	0.10	0.09	0.13	0.12	0.13	0.11	0.12	0.12

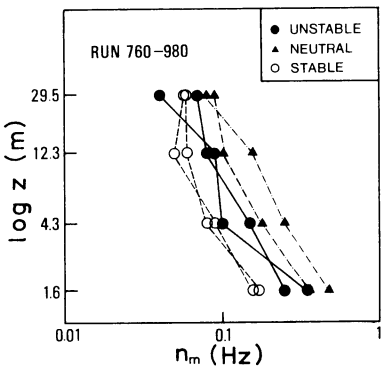

Fig. 4-14 Vertical profiles of the frequency n_m at which $nS_w(n)$ is a maximum. Symbols are the same as those in Fig. 4-1.

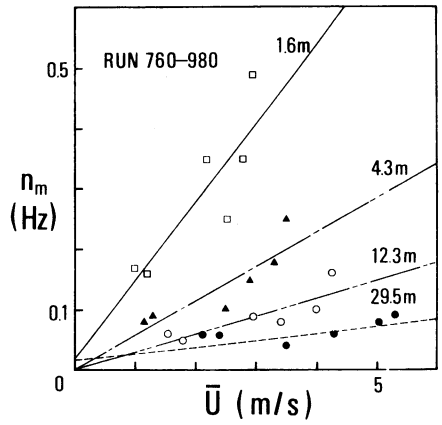

Fig. 4-15 Relationships between n_m and $\bar{U}$ at the four levels of the tower. Symbols are the same as those in Fig. 4-4.

1974) and the available estimates are collected in Table 4-5, where the wavelength $\lambda_m = \bar{U}/n_m$ is tabulated as ratio to the height z. Fig. 4-16 shows a plot of λ_m against z. For neutral conditions most of λ_m/z are between 2 and 4 (Table 4-4). This is in accordance with the previous studies by other investigators (Pasquill, 1974).

To enable comparison with other atmospheric and laboratory data, we apply the Monin-Obukhov similarity theory to the spectra. Each spectrum $nS_i(n)$ (i = u,w) was divided by the

Table 4-5 Comparison of the spectral scale λ_m of the vertical component with other results under neutral conditions

Reference	z (m)	Near-neutral λ_m/z
Panofsky and McCormick, 1954	91	3
Panofsky and McCormick, 1960	0.2 – 600	4
Smith, F.B., 1961	150, 600	2
Pasquill and Butler, 1964	2	3 – 3.5
Busch and Panofsky, 1968	3 – 137	3
Miyake et al., 1970	1.4 – 4.5	4
Kaimal et al., 1972	5.7 – 22.6	2
This study	1.6 – 29.5	3.3

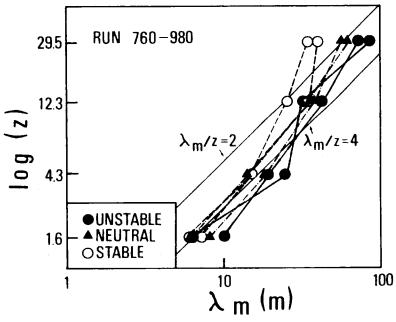

Fig. 4-16 Vertical profiles of the spectral scale λ_m. Symbols are the same as those in Fig. 4-1. The diagonal lines correspond to λ_m/z = 2 or 4.

variance σ_i^2 (i = u, w), and the n-scale was converted to a f-scale; the nondimensional frequency f is expressed as follows:

$$f = nz/\bar{U} \quad \ldots\ldots\ldots\ldots\ldots\ldots\ldots\ldots\ldots\ldots\ldots\ldots\ldots\ldots\ldots\ldots\ldots\ldots \quad (4\text{-}9)$$

According to the similarity theory such normalized spectra may be functions of both the stability parameter z/L and the non-dimensional frequency f:

$$nS_i(n)/\sigma_i^2 = G_{s,i}(f, z/L),\ i = u, w \quad \ldots\ldots\ldots\ldots\ldots\ldots\ldots\ldots\ldots\ldots \quad (4\text{-}10)$$

where $G_{s,i}$ is the universal function of the spectra. In Fig. 4-17 the normalized spectra of u and w at the four levels of the tower are shown against f. The straight lines have a slope of -2/3 corresponding to Kolmogorov's -5/3 power law. These spectral curves show the same general characteristics as found by other investigators, in particular the -2/3 slope on the high-frequency side. Stability effects can be seen in the figure; the spectral peak shifts to high frequencies as increasing stability. The values for the spectral peak f_m in Table 4-4 are between 0.2 and 0.8. f_m has a tendency to shift toward higher values of f as the height increases.

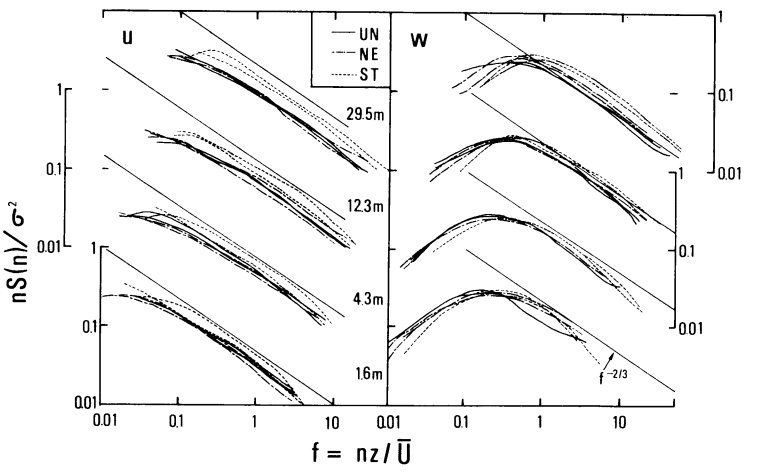

Fig. 4-17 Normalized spectra of the velocity components, $nS_i(n)/\sigma_i^2$ (i = u, w) at the four levels of the tower. The solid curves (——) show unstable conditions, the chain curves (—·—) neutral conditions, and the broken curves (- - - -) stable conditions.

4-2 Turbulent energy budget

At first, the variations of the turbulent energy budget with height and time will be shown in this section. Next, the behavior of each term in the budget equation of turbulent energy will be examined in relation to stability and other parameters. Finally, a model of the turbulent energy budget will be presented by means of the Monin-Obukhov similarity theory. The results will be discussed in comparison with previous studies (Wyngaard and Coté, 1971; McBean and Elliott, 1975; Garratt, 1972).

The values for each term in the budget equation were evaluated in the following six layers;

(1) a layer between the levels of 1.6 and 4.3 m

(2) a layer between the levels of 4.3 and 12.3 m

(3) a layer between the levels of 12.3 and 29.5 m

(4) a layer between the levels of 1.6 and 12.3 m

(5) a layer between the levels of 4.3 and 29.5 m

(6) the whole layer between the levels of 1.6 and 29.5 m

a) Vertical structure of the turbulent energy budget

Each term in the budget equation of turbulent energy (3-25) was computed for the data runs, and examples are shown in Fig. 4-18 for unstable conditions and Fig. 4-19 for stable conditions.

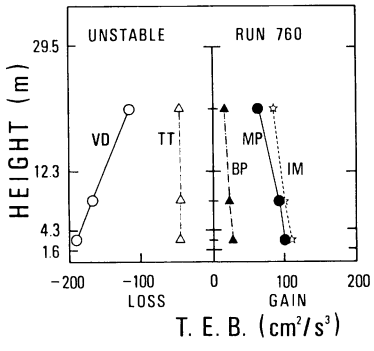

Fig. 4-18 Vertical structure of the turbulent energy budget in unstable conditions.

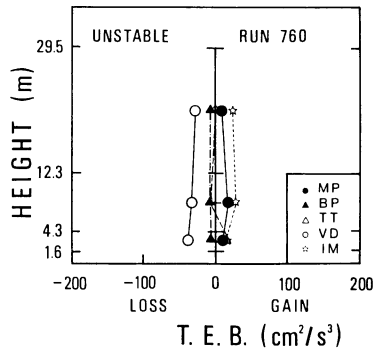

Fig. 4-19 As in Fig. 4-18 except for stable conditions.

From Fig. 4-18, it is clear that for unstable conditions buoyant production and turbulent transport are approximately balanced, and also mechanical production decreases with increasing height and the absolute value of viscous dissipation decreases with height. Mechanical and buoyant productions are sources of turbulent energy. The former is much larger than the latter in the surface boundary layer. Viscous dissipation and turbulent transport are energy sinks. The fact that turbulent transport is an energy sink means that near the surface, energy is exported upward by turbulence at double the rate it is produced by buoyancy. Viscous dissipation and mechanical production decrease markedly with height. This is caused by the effect of the surface boundary.

For stable conditions, each term of the turbulent energy budget is very small as compared with that for unstable conditions, and is almost constant with height (Fig. 4-19). Mechanical production is the only energy source and the others energy sinks.

It can be concluded from Fig. 4-18 and Fig. 4-19 that mechanical production and viscous dissipation are a main energy source and sink, respectively. They decrease with height. Turbulent transport is an energy sink to approximately balance buoyant production which may be a source or sink depending on stability. For stable conditions, the magnitude of each term is very small and almost constant with height.

In Fig. 4-20, the result for unstable conditions is compared with data from Lenschow (1970), who provided the vertical structure of the turbulent energy budget from 100 to 1,000 m above the surface. In contrast to the budget in the surface boundary layer, buoyant production is a main source of turbulent energy in the planetary boundary layer. Mechanical production is less important than the other terms. Turbulent transport increases with height to have a positive value above 500 m. This is expected because the energy exported from the lower layer has to appear as a local

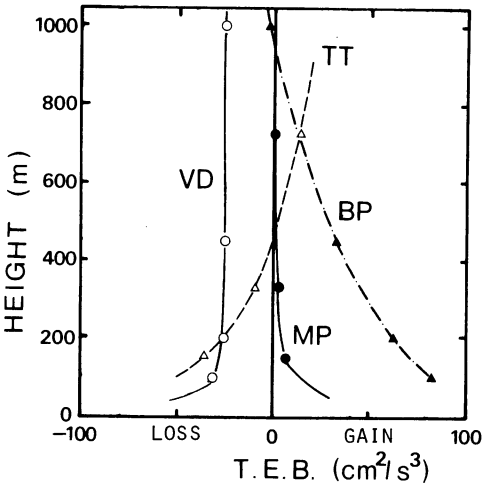

Fig. 4-20 Vertical structure of the turbulent energy budget in the planetary boundary layer (from Lenschow, 1970).

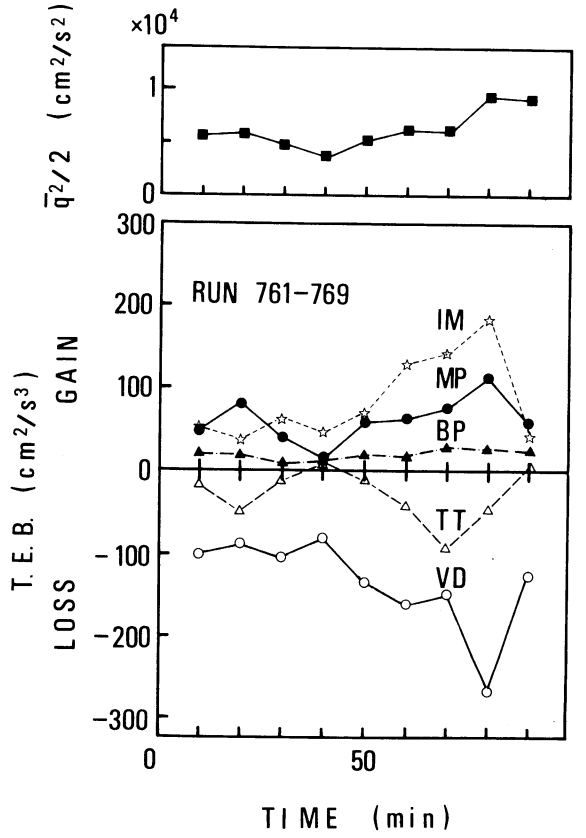

Fig. 4-21 Time change of each term in the budget equation of turbulent energy in unstable condtions.

import at the upper layer. Viscous dissipation is almost constant with height above 200 m.

b) Time change of the turbulent energy budget

Each term in the budget equation of turbulent energy (3-25) was computed for 9 consecutive 10-min blocks of data, and an example is shown in Fig. 4-21 for unstable conditions. The budget in the figure shows one within the layer between the levels of 1.6 and 12.3 m. Turbulent energy is also plotted against time.

As can be seen in Fig. 4-21, mechanical production appears to correspond to viscous dissipation. The magnitudes of these two terms tend to increase with turbulent energy. Buoyant production and turbulent transport are generally of similar magnitude.

By comparison, the time change of the budget within the upper layer between 50 and 150 m is shown in Fig. 4-22 obtained by Rayment and Caughey (1977). In contrast to the budget for the surface boundary layer, mechanical production is less important than other terms, and buoyant production is a main source of turbulent energy.

Fig. 4-23 shows the time change of the turbulent energy budget in the course of the destruction of the inversion layer. Fig. 4-24 shows the isopleths of mean wind speed and temperature for this case. When the inversion is well developed, the mean wind speed is very small. During the inversion, each term in the budget is very small, but increases in magnitude while the inversion breaks down.

c) Model of the turbulent energy budget

The budget equation of turbulent energy (3-25) can be made dimensionless through multiplication by kz/u_*^3 to obtain Eq. (3-26). The results are presented in dimensionless form, and kz/u_*^3 is used as a normalizing factor. Since all terms are normalized with the same factor, their relative magnitudes are unchanged. In all cases we refer to the terms on the left of Eq. (3-26), and if a term represents an energy gain, it is positive. The values for each term in Eq. (3-26) were evaluated in the previously-mentioned six layers.

We now proceed to a discussion of the behavior of the terms in Eq. (3-26) at all stabilities.

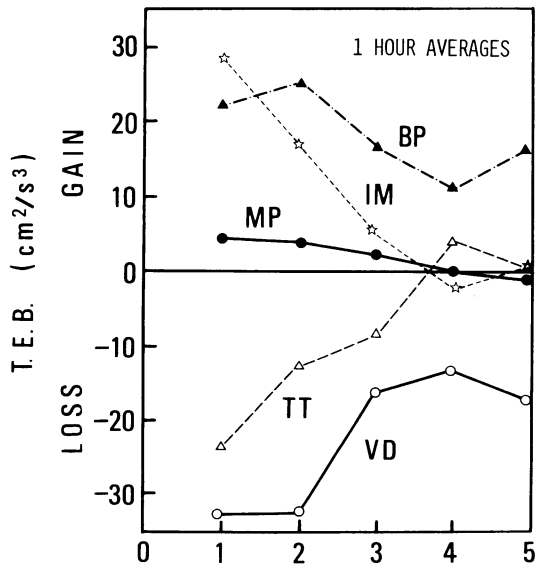

Fig. 4-22 Time change of each term in the budget equation of turbulent energy in the planetary boundary layer (from Rayment and Caughey, 1977).

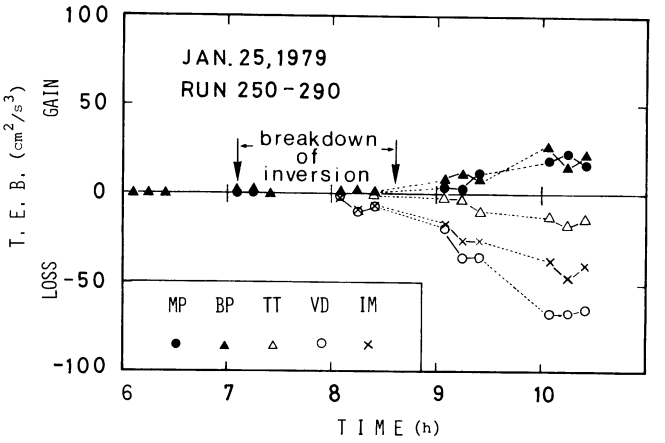

Fig. 4-23 Time change of each term in the budget equation of turbulent energy during the breakdown of the inversion.

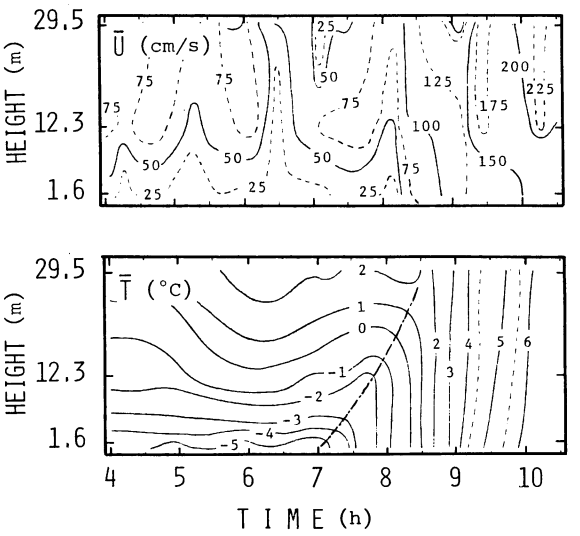

Fig. 4-24 Time change of mean wind speed and temperature during the breakdown of the inversion.

The results are summarized by the Monin-Obukhov similarity theory for comparison with previous studies.

(1) Viscous dissipation

Viscous dissipation is most important among the terms in the budget equation. As mentioned above, the estimates of viscous dissipation were obtained by assuming that Kolmogorov's hypothesis was valid, i.e.,

$$\epsilon_i = \left\{ \frac{S_i(\kappa)\kappa^{5/3}}{A_i} \right\}^{3/2}, \quad i = u, v, w \qquad \text{(4-11)}$$

for a range of wavenumber κ in the inertial subrange. The -5/3 power law was fitted to u, v, w spectra and ϵ is evaluated for each with $A_u = 0.50$ and $A_v = A_w = 0.67$ (Haugen, 1973). Fig. 4-25 compares the estimate ϵ_u obtained from the u spectrum with the estimate ϵ_w from the w spectrum. As can be seen in the figure, the agreement between ϵ_u and ϵ_w is good, so that ϵ_u is used as the estimate of ϵ.

Fig. 4-26 shows the vertical profiles of viscous dissipation, classified into three cases of unstable, neutral and stable conditions. For unstable and neutral conditions, viscous dissipation decreases with height.

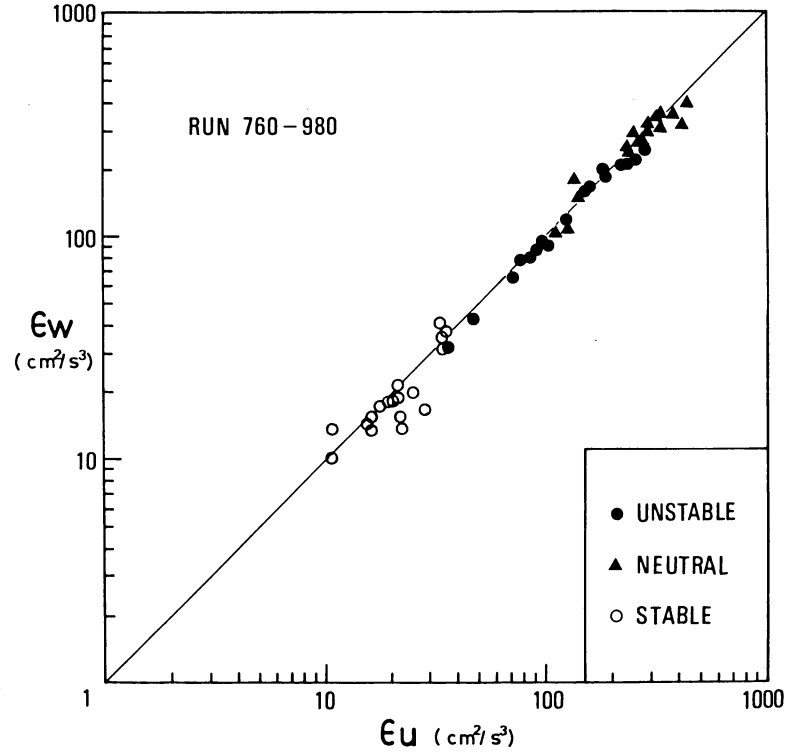

Fig. 4-25 Comparison of the estimate of viscous dissipation obtained by the u spectrum in the inertial subrange with that obtained by the w spectrum.

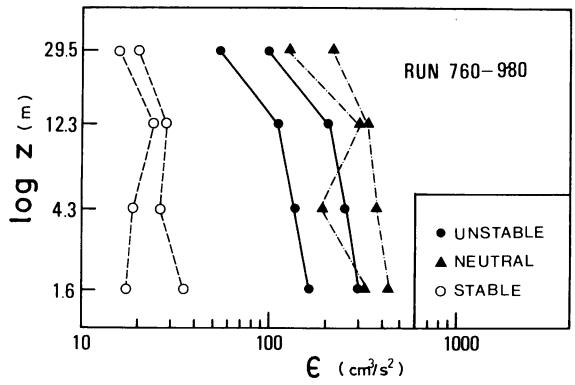

Fig. 4-26 Vertical profiles of viscous dissipation in unstable, neutral and stable conditions. Symbols are the same as those in Fig. 4-1.

Fig. 4-27 shows viscous dissipation as a function of mean wind speed at the four levels. From the figure, viscous dissipation increases with the third power of mean wind speed at a given height, but decreases with increasing height along the tower. The relation between ϵ and $\bar{U}$ at each level is expressed as follows:

$$\begin{aligned} \epsilon &= 16.5\ \bar{U}^3 \text{ at } 1.6 \text{ m} \\ \epsilon &= 8.3\ \bar{U}^3 \text{ at } 4.3 \text{ m} \\ \epsilon &= 4.7\ \bar{U}^3 \text{ at } 12.3 \text{ m} \\ \epsilon &= 1.2\ \bar{U}^3 \text{ at } 29.5 \text{ m} \end{aligned} \quad \cdots\cdots\cdots\cdots\cdots\cdots\cdots\cdots\cdots\cdots \quad (4\text{-}12)$$

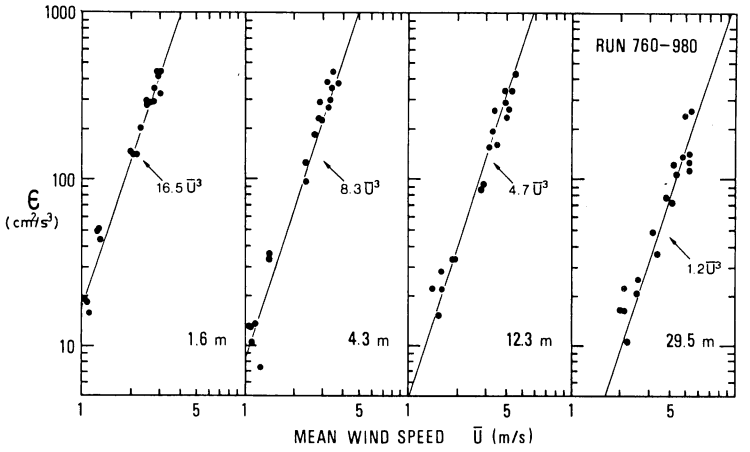

Fig. 4-27 Viscous dissipation as a function of mean wind speed at the four levels of the tower.

Assuming the neutral case of Eq. (3-25), the following equation may be obtained:

$$\epsilon = \frac{u_*^3}{kz}\,\phi_M(z/L) \quad \cdots\cdots\cdots\cdots\cdots\cdots\cdots\cdots\cdots\cdots\cdots\cdots \quad (4\text{-}13)$$

where ϕ_M is a function of stability z/L, and is unity when $z/L = 0$. Fig. 4-28 shows the relationship between ϵ and u_*^3/kz. It may be seen that there is some scatter in the figure because of the difference of stability, but a one-to-one relationship exists between ϵ and u_*^3/kz for the cases of near neutral conditions.

In order to examine the scatter seen in Fig. 4-28, ϵ normalized by u_*^3/kz is plotted against stability z/L in Fig. 4-29. The solid curve is fitted to the data, and the dashed curve was obtained by Wyngaard and Coté (1971). The curve fitted through the unstable data has the form

$$\phi_\epsilon(z/L) = (1 + 1.4|z/L|^{2/3})^{3/2} \quad \cdots\cdots\cdots\cdots\cdots\cdots\cdots\cdots \quad (4\text{-}14)$$

The curve had been assumed to go through 1.0 at the origin, in keeping with traditional thinking. The curve fitted through the stable data has the form

$$\phi_\epsilon(z/L) = \{1 + 2.2(z/L)^{3/5}\}^{3/2} \quad \cdots\cdots\cdots\cdots\cdots\cdots\cdots\cdots \quad (4\text{-}15)$$

The other investigators proposed the equations for viscous dissipation as follows:

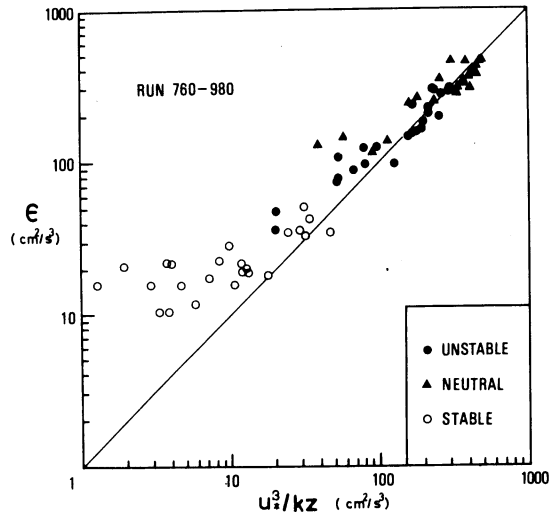

Fig. 4-28 Comparison of the measured viscous dissipation ϵ under various stabilities with the mechanical production of turbulent energy for neutral conditions, u_*^3/kz. Symbols are the same as those in Fig. 4-1.

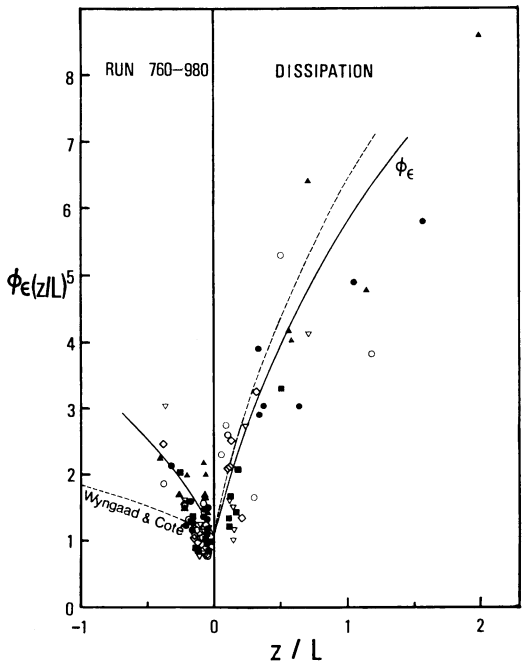

Fig. 4-29 Dimensionless viscous dissipation plotted against the stability parameter z/L. Symbols represent different layers as follows:

■ = 1.6 – 4.3 m, ◇ = 4.3 – 12.3 m,
▲ = 12.3 – 29.5 m, ▽ = 1.6 – 12.3 m,
○ = 4.3 – 29.5 m, ● = 1.6 – 29.5 m.

Wyngaard and Coté (1971)

$$\phi_\epsilon(z/L) = (1 + 0.5|z/L|^{2/3})^{3/2} \quad (z/L < 0)$$
$$= \{1 + 2.5(z/L)^{3/5}\}^{3/2} \quad (z/L > 0) \quad \ldots\ldots\ldots\ldots\ldots (4\text{-}16)$$

Busch and Panofsky (1968)

$$\phi_\epsilon(z/L) = 1 + 9z/L \quad (z/L > 0) \quad \ldots\ldots\ldots\ldots\ldots\ldots\ldots\ldots (4\text{-}17)$$

Garratt (1972)

$$\phi_\epsilon(z/L) = (1 - 16z/L)^{-1/4} - z/L \quad (z/L < 0)$$
$$= 1 + 4z/L \quad (z/L > 0) \quad \ldots\ldots\ldots\ldots\ldots (4\text{-}18)$$

Results for viscous dissipation in this study are generally consistent with the previous results, and the departures from them may be due to the differences of surface roughness.

(2) Mechanical production

Measurements of the dimensionless rate of mechanical production are shown in Fig. 4-30. The average properties of this curve should be those of the dimensionless wind shear $\phi_M(z/L)$, where

$$\phi_M(z/L) = \frac{kz}{u_*}\frac{\partial \bar{U}}{\partial z} \quad \ldots\ldots\ldots\ldots\ldots\ldots\ldots\ldots\ldots\ldots (4\text{-}19)$$

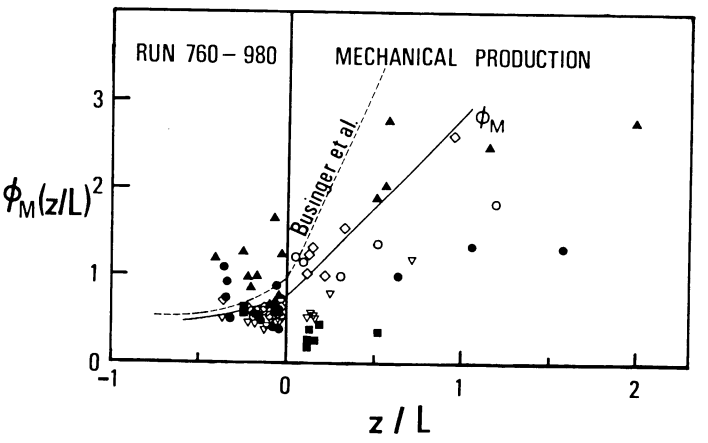

Fig. 4-30 Dimensionless rate of mechanical production of turbulent energy plotted against the stability parameter z/L. Symbols are the same as those in Fig. 4-29.

The curve fitted through the unstable data has the form

$$\phi_M(z/L) = (1 - 7z/L)^{-1/4} - 0.2 \quad \ldots\ldots\ldots\ldots\ldots\ldots (4\text{-}20)$$

Under stable conditions, the form of the curve is

$$\phi_M(z/L) = 0.8 + 2z/L \quad \ldots\ldots\ldots\ldots\ldots\ldots\ldots\ldots (4\text{-}21)$$

These interpolation formulas are shown in Fig. 4-30 as well as those obtained by Businger et al. (1971).

(3) Buoyant production

Buoyant production is simply normalized as

$$\phi_B(z/L) = -z/L \quad \cdots\cdots\cdots\cdots\cdots\cdots\cdots\cdots\cdots\cdots \quad (4\text{-}22)$$

and is a gain under unstable conditions and a loss under stable conditions.

(4) Turbulent transport

Turbulent fluctuations in the atmosphere act to transfer vertically turbulent energy in addition to momentum and heat. In this section we examine the flux of turbulent energy and its divergence, or turbulent transport.

Fig. 4-31 shows the vertical profiles of the flux of turbulent energy, $\overline{wq^2}/2$, for unstable, neutral and stable conditions. As can be seen in the figure, the vertical variation of $\overline{wq^2}/2$ between the lower levels (1.6 – 4.3 m) is rather small, but at the upper levels $\overline{wq^2}/2$ increases with height. The fact that the values for upper levels are larger than those for the lower levels indicates that turbulent energy produced in the lower layer is transported to the upper levels. This trend is striking for unstable and neutral conditions, but $\overline{wq^2}/2$ is almost constant with height for stable conditions.

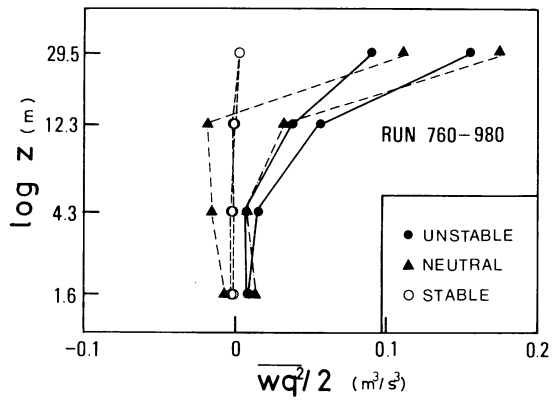

Fig. 4-31 Vertical profiles of the flux of turbulent energy in unstable, neutral and stable conditions. Symbols are the same as those in Fig. 4-1.

Fig. 4-32 shows the relation between $\overline{wq^2}/2$ and u_* for the case of $\overline{wq^2}/2 > 0$. This shows that $\overline{wq^2}/2$ increases rapidly with the third power of u_*.

The dimensionless flux of turbulent energy $\overline{wq^2}/2u_*^3$ is plotted against the stability parameter z/L in Fig. 4-33. The results show a marked trend with z/L for unstable conditions, though there is no trend is stable conditions. The flux of turbulent energy is positive in most unstable cases. This feature implies upward energy transport, particularly in unstable conditions. In Fig. 4-33, the results are compared with the results from three other studies: the data of Garratt (1972) plotted here are the sums of $\overline{w(u^2 + w^2)}/2u_*^3$ against z/L. Garratt did not measure the lateral component. The results of Wyngaard and Coté (1971) imply a curve of $\overline{wq^2}/2u_*^3 = -2.5\ z/L + B$, where B is not given. The third data set by Banke and Smith (1973) was collected over arctic sea

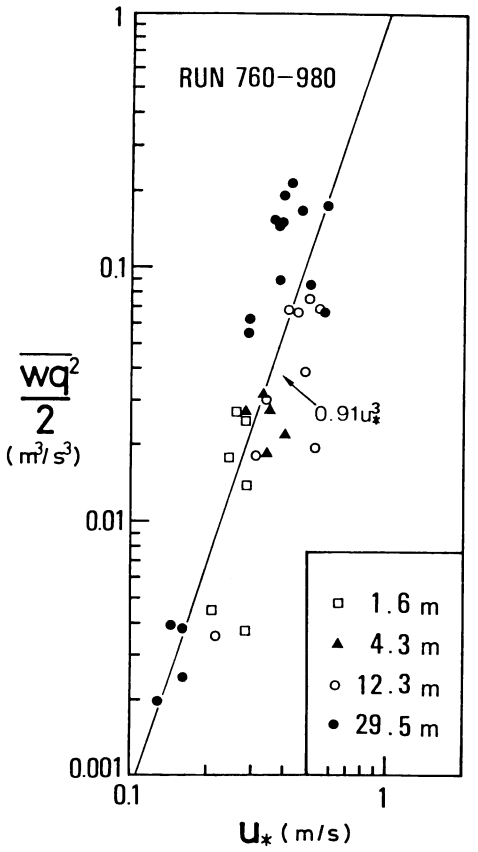

Fig. 4-32 Flux of turbulent energy plotted against the friction velocity. Symbols are the same as those in Fig. 4-4.

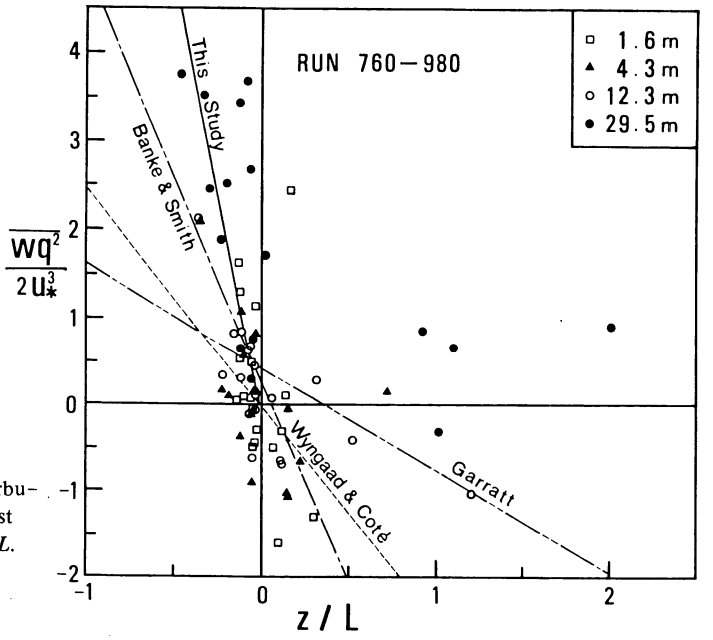

Fig. 4-33 Dimensionless flux of turbulent energy plotted against the stability parameter z/L. Symbols are the same as those in Fig. 4-4.

ice. The difference in slopes is partially a reflection of the different range of z/L used for linear regression.

Turbulent transport (flux divergence of turbulent energy) were estimated by approximating the vertical derivative of $\overline{wq^2}/2$. The results show some evidence of obeying similarity on the unstable side, although the scatter is large (Fig. 4-34). The solid line in the figure is a fit to the data on the unstable side. For unstable conditions, turbulent transport behaves approximately as

$$\phi_T(z/L) = 2\frac{z}{L} \quad \cdots\cdots\cdots\cdots\cdots\cdots\cdots\cdots\cdots\cdots\cdots\cdots\cdots\cdots \quad (4\text{-}23)$$

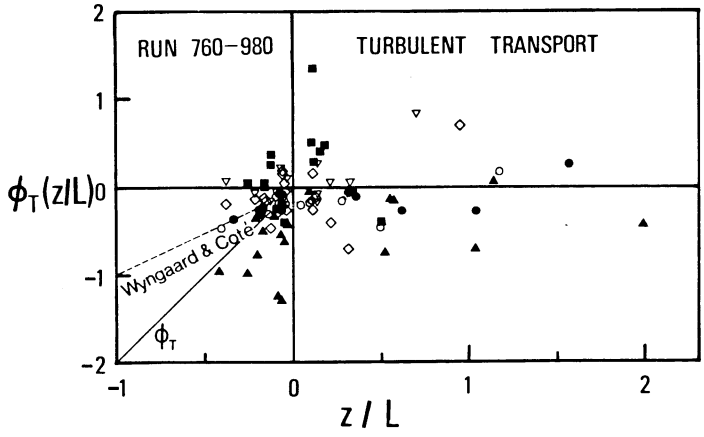

Fig. 4-34 Dimensionless rate of turbulent transport of turbulent energy plotted against the stability parameter z/L. Symbols are the same as those in Fig. 4-29.

Some of the scatter in the figure is probably due to the crude derivative approximation. Also, part of the scatter is probably caused by the inherently large uncertainty in the third moments; the statistical reliability of any estimate of a turbulent property will decrease, for a given averaging time, as the order of the property increases.

Turbulent transport on the stable side of Fig. 4-34 does not show any clear trend. There is scatter around zero for small z/L. At large z/L, almost all the estimates are smaller in magnitude than z/L. It appears that turbulent transport is small compared to the dominant terms in the budget of turbulent energy.

(5) The imbalance

Fig. 4-35 shows the dimensionless imbalance term as a function of z/L. As can be seen from the figure, the imbalance is zero for near neutral conditions ($z/L \cong 0$). As the magnitude of z/L increases, the imbalance becomes considerably larger. The curve fitted to the data on the unstable side is

$$\phi_I(z/L) = (1 + 0.5|z/L|^{2/3})^{3/2} - 1 \quad \cdots\cdots\cdots\cdots\cdots\cdots\cdots\cdots\cdots\cdots \quad (4\text{-}24)$$

and the curve on the stable side is

$$\phi_I(z/L) = \{1 + 2.4(z/L)^{3/5}\}^{3/2} - 1 \quad \cdots\cdots\cdots\cdots\cdots\cdots\cdots\cdots\cdots\cdots \quad (4\text{-}25)$$

Several factors arise as possible contributors to the imbalance. Firstly, it is recognized that any

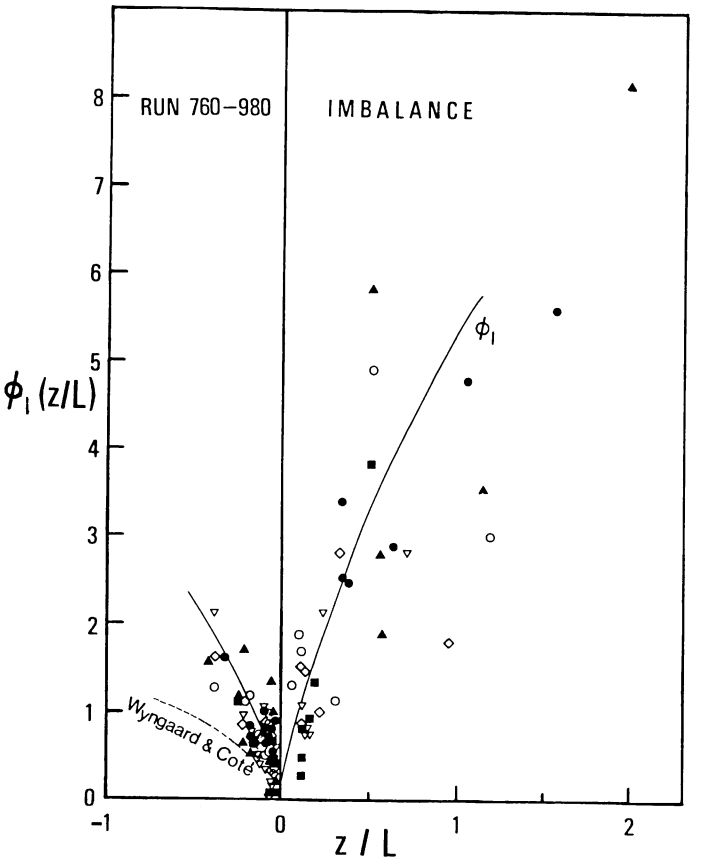

Fig. 4-35 Dimensionless imbalance of the turbulent energy budget plotted against the stability parameter z/L. Symbols are the same as those in Fig. 4-29.

budget term found by difference contains the accumulated errors of the measured terms, which show scatter about their fitted curves. Buoyant production, a second moment measured at a point, shows the least scatter and is accurate. Turbulent transport, a spatial derivative of a third moment, shows the most scatter and its fitted curve is least certain.

For very stable conditions, the imbalance shows to be a large gain. The stable dissipation could be overestimated, and the mechanical production could be underestimated because of a relatively crude estimation of the vertical derivative of mean wind speed. These errors could account for most of the imbalance under stable conditions.

For very unstable conditions, the unmeasured terms, those reflecting possible horizontal inhomogeneity and pressure transport, would naturally be suspected of causing the imbalance.

(6) Model

The model of the turbulent energy budget was deduced from the results. Fig. 4-36 shows the trend lines of all terms in the budget equation against z/L. In neutral conditions, mechanical production and viscous dissipation are approximately in balance, while turbulent transport and buoyant production are not important. The imbalance is zero. In unstable conditions, each term

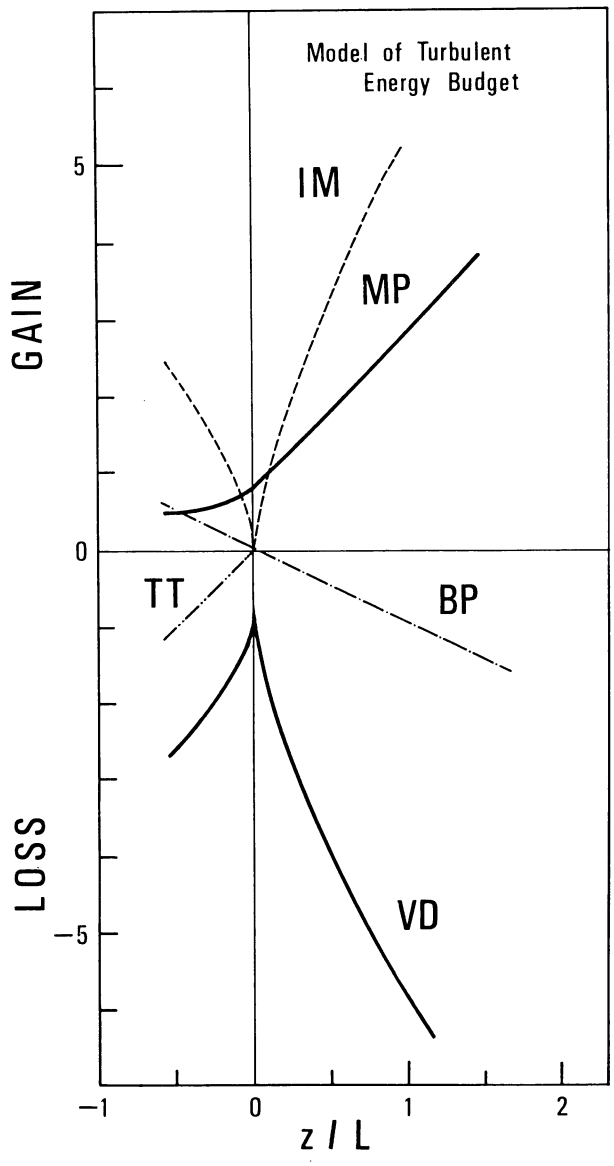

Fig. 4-36 A proposed model of the turbulent energy budget.

in the budget equation is significant, and buoyant production is a gain. In this case the imbalance increases with the magnitude of absolute stability. Mechanical production becomes less important as instability increases, and buoyant production assumes a dominant role as the energy source. In addition, energy is exported upward by turbulence (turbulent transport) at double the rate it is produced by buoyancy. In stable conditions, all terms except turbulent transport are significant, and buoyant production is a loss. For both stable and unstable conditions, the imbalance increases with the magnitude of absolute stability.

The general features of the model for unstable conditions correspond approximately to those in Fig. 1-2, which was obtained by Wyngaard and Coté (1971). Some departures from them may

be due to the difference of roughness of the surface. For very unstable and stable conditions, the unmeasured terms, which reflect possible horizontal inhomogeneity and pressure transport, would be suspected of causing the imbalance.

CHAPTER 5

CONCLUSIONS

Turbulence measurements of wind and temperature were made by sonic anemometer-thermometers in the first thirty meters of the atmosphere. This experiment has allowed a detailed study of the turbulent energy budget as well as turbulence statistics in this layer.

Turbulence statistics were analyzed and interpreted in relation to measured parameters, such as height, mean wind speed and stability conditions. Summarizing the results for turbulence statistics, the following features are shown:

(1) The values for the friction velocity u_* at four levels of the tower increase linearly with the mean wind speed $\bar{U}$.

(2) The standard deviations of the velocity components, σ_i ($i = u, v, w$) are closely related to the mean wind speed $\bar{U}$, the friction velocity u_* and the stability parameter z/L for the case of a stationary boundary layer. The data for the horizontal components u, v are rather scattered in comparison with one for the vertical component w.

(3) The ratios $\sigma_i/\bar{U}$ ($i = u, v, w$) at the upper levels are smaller than those at lower levels.

(4) The ratio σ_w/u_* shows a dependency on stability. The values agree well with the results by other investigators.

Spectral analysis of turbulent fluctuations shows the following features:

(5) The spectra of the velocity components on the high-frequency side have the slope of $-5/3$ corresponding to Kolmogorov's hypothesis; the $-5/3$ region is assumed to be the inertial subrange. The spectra of the longitudinal component u are found to obey the $-5/3$ power law at much lower frequencies than those of the vertical component w. The position of the inertial subrange shifts to lower frequencies as increasing height and stability. In the inertial subrange, the ratio between the spectra of u and w is 4/3.

(6) The magnitude of the spectra depends on both mean wind speed and stability. Under all conditions, the u spectra contain much more energy at low frequencies than the w spectra.

(7) The horizontal scale of turbulence is larger than the vertical one. The scale of turbulence increases with height and stability, and decreases with the mean wind speed.

(8) The peak frequency of the spectra, n_m has a close relation to the lower limit of the inertial subrange, $n_{i.s.}$. The ratio of the wavelength $\lambda_m = \bar{U}/n_m$ to the height z is between 2 and 4 and approximately constant with height in the surface boundary layer.

(9) The normalized spectra $nS_i(n)/\sigma_i^2$ ($i = u, w$) have the slope of $-2/3$ corresponding to Kolmogorov's $-5/3$ power law.

Each term in the budget equation of turbulent energy was estimated from the measurements of turbulence statistics and their profiles. The vertical structure and time change of the turbulent energy budget were examined and compared with the budget in the planetary boundary layer, obtained by other investigators. The estimates of viscous dissipation were obtained from the inertial-subrange levels of the spectra of the longitudinal velocity with a value of 0.50 for the spectral constant. The results are summarized as follows:

(10) For unstable conditions, mechanical production and viscous dissipation are a main energy source and sink, respectively. They decrease with height because of the surface boundary. Buoyant production is an energy source, and is smaller than mechanical production in the surface boundary layer. Turbulent transport is an energy sink. This means that near the surface, turbulent energy is exported upward by turbulence.

(11) For stable conditions, each term of the budget is very small as compared with that for unstable conditions, and is almost constant with height. Mechanical production is the only energy source and the others energy sinks.

(12) The turbulent energy budget in the surface boundary layer is different from that in the planetary boundary layer, where buoyant production is a main source of turbulent energy. Mechanical production is less important than the other terms. Turbulent transport increases with height to have a positive value above 500 m from the ground. This is expected because the energy exported from the lower layer has to appear as a local import at the upper layer.

The behavior of each term in the budget equation of turbulent energy was examined in relation to stability and other parameters. The results are summarized as follows:

(13) Viscous dissipation increases with the third power of mean wind speed, and decreases with height. For near neutral conditions, viscous dissipation is balanced with mechanical production.

(14) The flux of turbulent energy has a positive value, and increases with height. This trend is obvious for neutral and unstable conditions, but the flux is almost constant with height for stable conditions. This fact indicates that the turbulent energy produced in the lower layer is transported to upper levels. The flux increases with the third power of friction velocity. The divergence of this flux, or turbulent transport shows some evidence of obeying similarity on the unstable side, although the scatter is large. Turbulent transport does not show any clear tendency on the stable side.

(15) The behavior of the imbalance can be expressed as a function of stability. The imbalance is zero for near neutral conditions. As the magnitude of stability increases, the imbalance becomes considerably larger. The imbalance may be attributed either to pressure transport (which was not measured) or to experimental difficulties such as horizontal inhomogeneity.

A model of the turbulent energy budget was deduced from the results. A general specification of turbulent energy budget including the case of stable conditions has been achieved through the present model. Under near neutral conditions, mechanical production and viscous dissipation are dominant and essentially in balance, while turbulent transport and buoyant production are not important. In unstable conditions, each term in the budget is important, and buoyant production is a gain. In stable conditions, all terms except turbulent transport are significant, while buoyant production is a loss. Mechanical production is the only source of turbulent energy and the others energy sinks. For both stable and unstable conditions the imbalance term increases with the magnitude of stability.

ACKNOWLEDGEMENTS

The author is grateful to Dr. M.M. Yoshino of the Institute of Geoscience for many helpful suggestions and encouragement. The author is also grateful to Drs. T. Kawamura, T. Nishizawa, K. Kotoda and T. Hanafusa of the Institute of Geoscience for reviewing this paper. Frequent, stimulating and helpful discussions with Dr. Hanafusa are gratefully acknowledged. Thanks are due to Dr. M. Inokuchi, former Director of Environmental Research Center for making available the experiments on which this paper is based. Thanks are also due to Dr. H. Tamiya of the Meteorological Research Institute, Dr. Y. Sakura of Environmental Research Center and Mr. Y. Hayashi of the Institute of Geoscience for many helpful suggestions, Mr. T. Yorisaki and Miss H. Takeuchi for their help in the preparation of the experiment and data reduction. The author is indebted to Mrs. P. Ogawa for a critical reading of the manuscript and my wife for typing the manuscript and drawing the figures. The computations in the present study were performed with use of the ACOS-800 computer at the Science Information Processing Center. It is a great pleasure for me to thank my parents and my wife for their help, encouragement and understanding during the entire course of this work.

REFERENCES

Banke, E.G. and Smith, S.D. (1973): Wind stress on arctic sea ice. *J. Geophys. Res.*, **78**, 7871-7883.

Busch, N.E. and Panofsky, H.A. (1968): Recent spectra of atmospheric turbulence. *Quart. J. Roy. Met. Soc.*, **94**, 132-148.

Businger, J.A., Wyngaard, J.C., Izumi, Y. and Bradley, E.F. (1971): Flux-profile relationship in the atmospheric surface layer. *J. Atmos. Sci.*, **28**, 181-189.

Caughey, S.J. and Wyngaard, J.C. (1979): The turbulence kinetic energy budget in convective conditions. *Quart. J. Roy. Met. Soc.*, **105**, 231-239.

Champagne, F.H., Friehe, C.A. and LaRue, J.C. (1977): Flux measurements, flux estimation techniques, and fine-scale turbulence measurements in the unstable surface layer over land. *J. Atmos. Sci.*, **34**, 515-530.

Elliott, J.A. (1972): Instrumentation for measuring static pressure fluctuations within the atmospheric boundary layer. *Boundary-Layer Met.*, **2**, 476-495.

Garratt, J.R. (1972): Studies of turbulence in the surface layer over water (Lough Neagh) Part II. Production and dissipation of velocity and temperature fluctuations. *Quart. J. Roy. Met. Soc.*, **98**, 642-657.

Gifford, F.A. (1962): The vertical variation of atmospheric eddy energy dissipation. *J. Atmos. Soc.*, **19**, 205-206.

Haugen, D.A. (ed.), (1973): *Workshop on micrometeorology.* American Meteor. Soc., 392pp.

Hino, M. (1977): *Spectral analysis (in Japanese).* Asakura Shoten, Tokyo, 300pp.

Hinze, J.O. (1959): *Turbulence.* McGraw-Hill, 586pp.

Ito, S. (1969): A mechanism of turbulent transfer in the atmospheric surface layer. *J. Met. Soc. Japan,* **47**, 419-430.

Ito, S. (1972): On a similarity rule for the geophysical flow with the thermal stratification. *J. Met. Soc. Japan,* **50**, 229-233.

Izumi, Y. and Malad, M.L. (1970): Wind speeds as measured by cup and sonic anemometers and influenced by tower structure. *J. Appl. Met.*, **9**, 851-856.

Jenkins, G.M. and Watts, D.G. (1968): *Spectral analysis and its applications.* Holden-Day, San Francisco, 525pp.

Kai, K. (1976): *Three-components analysis of turbulence spectra in the surface boundary layer.* M.S. Thesis, Tokyo Kyoiku Univ., 63pp.

Kai, K. (1978): Measurements of turbulent characteristics at the ERC 30-m meteorological tower and data processing. *Bull. Envir. Res. Center (Univ. of Tsukuba),* **2**, 25-36.

Kai, K. (1980): On the characteristics of turbulence statistics and the budget of turbulent energy in the surface boundary layer. *Bull. Envir. Res. Center (Univ. of Tsukuba),* **4**, p100.

Kaimal, J.C., Wyngaard, J.C., Haugen, D.A., Coté, O.R. and Izumi, Y. (1976): Turbulence structure in the convective boundary layer. *J. Atmos. Sci.,* **33**, 2152-2169.

Kaimal, J.C., Haugen, D.A. and Newman, J.T. (1977): A computer-controlled mobile micrometeorological observation system. *J. Appl. Met.,* **5**, 411-420.

Karacostas, T.S. and Marwitz, J.D. (1980): Turbulent kinetic energy budgets over mountainous terrain. *J. Appl. Met.,* **19**, 163-174.

Kotoda, K., Sakura, Y., Hayashi, Y. and Kai, K. (1978): On the observation and data acquisition system for the heat and water balance studies of ERC experimental field. *Bull. Envir. Res. Center (Univ. of Tsukuba),* **2**, 65-89.

Lenschow, D.H. (1970): Airplane measurements of planetary boundary layer structure. *J. Appl. Met.,* **9**, 874-884.

Lenschow, D.H. (1974): Model of the height variation of the turbulent kinetic energy budget in the unstable planetary boundary layer. *J. Atmos. Sci.,* **31**, 465-474.

Lumley, J.L. and Panofsky, H.A. (1964): *The structure of atmospheric turbulence.* John Wiley & Sons, Inc., 239pp.

Maitani, T. (1977): Vertical transport of turbulent kinetic energy in the surface layer over a paddy field. *Boundary-Layer Met.,* **12**, 406-423.

McBean, G.A. (1970): *The turbulent transfer mechanisms in the atmospheric boundary layer.* Ph. D. Thesis, University of British Columbia.

McBean, G.A. (1978): The energy budgets of the turbulent velocity components and velocity-pressure gradient interactions. *J. Atmos. Sci.,* **35**, 1890-1899.

McBean, G.A., Stewart, R.W. and Miyake, M. (1971): The turbulent energy budget near the surface. *J. Geophys. Res.,* **76**, 6540-6549.

McBean, G.A. and Elliott, J.A. (1975): The vertical transports of kinetic energy by turbulence and pressure in the boundary layer. *J. Atmos. Sci.,* **32**, 753-766.

Mitsuta, Y. (1966): Sonic anemometer-thermometer for general use. *J. Met. Soc. Japan,* **44**, 1-24.

Mitsuta, Y. (1971): Sonic anemometer-thermometer and its application to the study of atmospheric boundary layer. *Tenki,* **18**, 377-385.

Miyake, M., Stewart, R.W. and Burling, R.W. (1970): Spectra and cospectra of turbulence over water. *Quart. J. Roy. Met. Soc.,* **96**, 138-143.

Monin, A.S. and Obukhov, A.M. (1954): Basic laws of turbulent mixing in the ground layer of the atmosphere. *Tr. Geofiz. Inst. Akad. Nauk SSSR,* **151**, 163-187.

Monin, A.S. and Yaglom, A.M. (1971): *Statistical fluid mechanics of turbulence.* The MIT Press, 769pp.

Monji, N. (1973): Budgets of turbulent energy and temperature variance in the transition zone from forced to free convection. *J. Met. Soc. Japan,* **51**, 133-145.

Monji, N. and Businger, J.A. (1972): Stability dependence of temperature, humidity and vertical wind velocity variances in the atmospheric surface layer. *J. Met. Soc. Japan,* **50**, 122-130.

Munn, R.E. (1966): *Descriptive micrometeorology.* Academic Press, 235pp.

Naito, G. (1978): Direct measurements of momentum and sensible heat fluxes at the tower in the open sea. *J. Met. Soc. Japan,* **56**, 25-34.

Obukhov, A.M. (1946): Turbulence in an atmosphere with inhomogeneous temperature. *Tr. Inst. Teoret. Geofiz. Akad. Nauk SSSR,* **1**, 95-115.

Ogura, Y. and Asai, T. (1975): *Kaiyo Kisho (Marine Meteorology).* Univ. of Tokyo Press, 191pp.

Panofsky, H.A. (1962): The budget of turbulent energy in the lowest 100 meters. *J. Geophys. Res.,* **67**, 3161-3165.

Panofsky, H.A. and McCormick, R.A. (1954): Properties of spectra of atmospheric turbulence at 100 meters. *Quart. J. Roy. Met. Soc.,* **80**, 546-564.

Panofsky, H.A. and McCormick, R.A. (1960): The spectrum of vertical velocity near the surface. *Quart. J. Roy. Met. Soc.,* **86**, 495-503.

Panofsky, H.A., Tennekes, H., Lenschow, D.H. and Wyngaard, J.C. (1977): The characteristics of turbulent velocity components in the surface layer under convective conditions. *Boundary-Layer Met.,* **11**, 355-361.

Pasquill, F. (1972): Some aspects of boundary layer description. *Quart. J. Roy. Met. Soc.,* **98**, 469-494.

Pasquill, F. (1974): *Atmospheric diffusion.* Ellis Horwood, 429pp.

Pasquill, F. and Butler, H.E. (1964): A note on determining the scale of turbulence. *Quart. J. Roy. Met. Soc.,* **90**, 79-84.

Plate, E.J. (1971): *Aerodynamic characteristics of atmospheric boundary layers.* U.S. Atomic Energy Commission, 190pp.

Pond, S., Smith, S.D., Hamblin, P.F. and Burling, R.W. (1966): Spectra of velocity and temperature fluctuations in the atmospheric boundary layer over the sea. *J. Atmos. Sci.,* **23**, 376-386.

Pond, S., Phelps, G.T., Paquin, J.E., McBean, G. and Stewart, R.W. (1971): Measurements of the turbulent fluxes of momentum, moisture and sensible heat over the ocean. *J. Atmos. Sci.,* **28**, 901-917.

Priestley, C.H.B. (1959): *Turbulent transfer in the lower atmosphere.* The Univ. of Chicago Press, 130pp.

Rayment, R. and Caughey, S.J. (1977): An investigation of the turbulence balance equations in the atmospheric boundary layer. *Boundary-Layer Met.,* **11**, 16-25.

Record, F.A., and Cramer, H.E. (1966): Turbulent energy dissipation rates and exchange processes above a nonhomogeneous surface. *Quart. J. Roy. Met. Soc.,* **92**, 519-532.

Schwerdtfeger, P. (1976): *Physical principles of micrometeorological measurements.* Elsevier Scientific Publishing Company, 113pp.

Sheppard, P.A., Tribble, D.T. and Garratt, J.R. (1972): Studies of turbulence in the surface layer over water (Lough Neagh) Part I. Instrumentation, programme, profiles. *Quart. J. Roy. Met. Soc.,* **98**, 627-641.

Shimanuki, A. (1973): Kyokaiso to Ranryu (Boundary layer and turbulence). *Met. Res. Note,* **114**, 1-69.

Sitaraman, V. (1970): Spectra and cospectra of turbulence in the atmospheric surface layer. *Quart. J. Roy. Met. Soc.,* **96**, 744-749.

Smith, F.B. (1961): An analysis of vertical wind fluctuations at heights between 500 and 5,000 feet. *Quart. J. Roy. Met. Soc.,* **87**, 180-193.

Sutton, O.G. (1953): *Micrometeorology.* McGraw-Hill Book Company, 333pp.

Tennekes, H. and Lumley, J.L. (1972): *A first course in turbulence.* The MIT Press, 300pp.

Wyngaard, J.C. (1978): Estimating momentum, heat and moisture fluxes from structure parameters. *J. Atmos. Sci.,* **35**, 1204-1211.

Wyngaard, J.C. and Coté, O.R. (1971): The budgets of turbulent kinetic energy and temperature variance in the atmospheric surface layer. *J. Atmos. Sci.*, **28**, 190-201.

Wyngaard, J.C. Coté, O.R. and Izumi, Y. (1971): Local free convection, similarity, and the budgets of shear stress and heat flux. *J. Atmos. Sci.*, **28**, 1171-1182.

Wyngaard, J.C. and Coté, O.R. (1972): Cospectral similarity in the atmospheric surface layer. *Quart. J. Roy. Met. Soc.*, **98**, 590-603.

Yamamoto, S., Yokoyama, O. and Gamo, M. (1979): Observational study on the turbulent structure of the atmospheric boundary layer under stable conditions. *J. Met. Soc. Japan*, **57**, 423-431.

Zubkovskiy, S.L. and Koprov, B.M. (1970): On the turbulent energy balance in the boundary layer of the atmosphere. *Izv. Atmos. Oceanic Phys.*, **6**, 589-592.

発行　　昭和57年3月10日
編集・発行者　筑波大学水理実験センター

〒305　茨城県新治郡桜村天王台1－1－1
TEL　0298(53)2532, 2534

印刷　日青工業株式会社
東京都港区西新橋2－5－10